

Nearby Spiral Galaxy Globular Cluster Systems II: Globular Cluster Metallicities in NGC 300^{1,2,3}

Julie B. Nantais and John P. Huchra

Harvard-Smithsonian Center for Astrophysics

60 Garden Street, Cambridge, MA 02138

Pauline Barmby

University of Western Ontario

London, ON N6A 3K7, Canada

and

Knut A. G. Olsen

Cerro-Tololo Inter-American Observatory, National Optical Astronomy Observatory

Casilla 603, La Serena, Chile

ABSTRACT

We present new metallicity estimates for globular cluster (GC) candidates in the Sd spiral NGC 300, one of the nearest spiral galaxies outside the Local Group. We have obtained optical spectroscopy for 44 Sculptor Group GC candidates with the Boller and Chivens (B&C) spectrograph on the Baade Telescope at Las Campanas Observatory. There are 2 GCs in NGC 253 and 12 objects in NGC 300 with globular-cluster-like spectral features, 9 of which have radial velocities above 0 km s^{-1} . The remaining three, due to their radial velocities being below

¹Data for this project were obtained at the Baade 6.5 m telescope, Las Campanas Observatory, Chile.

²This study uses observations from the Hubble Space Telescope obtained at the Space Telescope Science Institute, operated by the Association of Universities for Research in Astronomy, Inc., under NASA contract NAS 5-26555. These observations are associated with Programs GO-9162, GO-9492, and GO-10915.

³This publication makes use of data products from the Two Micron All Sky Survey, which is a joint project of the University of Massachusetts and the Infrared Processing and Analysis Center/California Institute of Technology, funded by the National Aeronautics and Space Administration and the National Science Foundation.

the expected 95% confidence limit for velocities of NGC 300 halo objects, are flagged as possible foreground stars. The non-clusterlike candidates included 13 stars, 15 galaxies, and an HII region. One GC, four galaxies, two stars, and the HII region from our sample were identified in archival Hubble Space Telescope images. For the GCs, we measure spectral indices and estimate metallicities using an empirical calibration based on Milky Way GCs. The GCs of NGC 300 appear similar to those of the Milky Way. Excluding possible stars and including clusters from the literature, the GC system (GCS) has a velocity dispersion of 68 km s^{-1} , and has no clear evidence of rotation. The mean metallicity for our full cluster sample plus one literature object is $[\text{Fe}/\text{H}] = -0.94$, lying above the relationship between mean GC metallicity and overall galaxy luminosity. Excluding the three low-velocity candidates, we obtain a mean $[\text{Fe}/\text{H}] = -0.98$, still higher than expected, raising the possibility of significant foreground star contamination even in this sample. Visual confirmation of genuine GCs using high-resolution space-based imagery could greatly reduce the potential problem of interlopers in small samples of GCSs in low-radial-velocity galaxies.

Subject headings: galaxies: star clusters: general—galaxies: individual (NGC 300)—galaxies: spiral

1. Introduction

Globular clusters (GCs), relics of some of the earliest and/or most violent phases of star and galaxy formation, can be analyzed to understand how various types of galaxies formed, as described in the review by Brodie and Strader (2006). Two subpopulations of GCs, metal-rich (red) and metal-poor (blue), exist in most early-type galaxies. Both are thought to be old, but the red metal-rich GCs are thought to be slightly younger (Larsen et al. 2001; Kundu and Whitmore 1998; Lee, Kim, and Geisler 1998). Large spiral galaxies, including the Milky Way (Zinn 1985) and Andromeda (Barmby et al. 2000), also have metal-rich and metal-poor GC subpopulations. In smaller, later-type galaxies, however, often only a metal-poor population is seen (Chandar et al. 2004).

The three basic models for bimodal GC system (GCS) formation in early type galaxies are dwarf galaxy accretion (Côté, Marzke, and West 1998), in situ formation (Forbes, Brodie, and Grillmair 1997), and gas-rich mergers (Ashman and Zepf 1992). In the last scenario, the original spiral galaxies — likely late-type spirals — would provide the entire metal-poor GC population, and the metal-rich GC population would form in the merger. Some evidence for GCs resulting from every one of these processes exists, but the properties of both blue and red GC popula-

tions have been found to scale with the mass of the host galaxy (Strader, Brodie, and Forbes 2004), indicating that the accretion model alone cannot account for the majority of blue GCs in bright galaxies. In any case, at high redshift and with a hierarchical merging scenario as the main process of galaxy formation, the distinction between these models fades.

The nearby Sculptor Group (or filament) is home to several late-type galaxies (Hubble types Sc–Im), including NGC 253 (the largest), NGC 300, NGC 55, and NGC 45. At a distance of 1.9 Mpc (Gieren et al. 2004), NGC 300 is one of the nearest spiral galaxies outside of the Local Group. As a nearby example of a late-type, midsize spiral galaxy, it is especially useful for understanding the sparse and thus relatively poorly studied GCSs of late-type galaxies. Kim et al. (2002) studied the star clusters in NGC 300 photometrically and identified 17 objects as GC candidates based on their size, shape, and color. Olsen et al. (2004) performed photometry on fields in six Sculptor Group galaxies and identified GC candidates via shape and color, and then obtained spectra for 19 GCs. Six of these spectroscopically confirmed clusters had high enough signal-to-noise spectra for metallicity determination via Lick/IDS indices. Seven of the GCs Olsen et al. spectroscopically confirmed were in NGC 300, and two had spectroscopically determined metallicities.

In this paper we present new metallicities derived from spectroscopy of GCs in Sculptor Group galaxies, primarily NGC 300, using Kim et al. (2002) and Olsen et al. (2004) as reference catalogs. We compare the metallicities of NGC 300 GCs to those of M31 and Milky Way clusters, and also determine NGC 300’s place on the galaxy luminosity-GCS metallicity relation of Brodie and Huchra (1991).

2. Data reduction and cluster selection

We obtained spectra of 44 Sculptor Group cluster candidates with the Boller & Chivers (B&C) spectrograph on the Baade telescope from 2002 November 6 to 2002 November 9. We chose to observe all 17 GC candidates from Kim et al. (2002), plus 25 Olsen et al. (2004) NGC 300 GC candidates with no previous spectra (except for NGC 300ax) observed in order of increasing magnitude from brightest to faintest. We also observed the two brightest unconfirmed Olsen et al. GC candidates in NGC 253. Nineteen of our 27 Olsen et al. cluster candidates are among the 38 Sculptor Group GC candidates for which we also obtained *JHK* photometry with the PANIC camera on the Baade 6.5 m telescope (Nantais et al. 2006, Paper I). Figure 1 shows the locations of the NGC 300 objects we observed with respect to a schematic of the NGC 300 disk.

The advantages of using the long-slit B&C spectrograph rather than a fiber spectrograph

are good coverage in blue optical wavelengths and better sky subtraction (due to the sky background being determined at the same time and place as the object exposure). Also, the sky at Las Campanas has significantly weaker telluric emission lines than less isolated telescope locations.

Our spectra were taken with the 600 l mm⁻¹ grating blazed at 5000 Å. The wavelength range is about 3700-6860 Å. Peak count rates occurred between 5000 and 5500 Å for objects with typical GC colors. The dispersion of the spectra is ~ 1.6 Å pixel⁻¹, and the resolution of the spectra is about 5 Å. The readout noise is 3.1 e⁻. Total exposure times were as low as 180 s for very bright objects and as high as 3600 s for faint objects, with 600-2400 s exposure times for most objects. Exposure times under 600 s were usually done as single exposures, while longer exposures were usually broken up into 2-4 exposures of 600-900 s each. Seeing ranged from 0.6-1.9'' over the course of observations, with 1'' being typical, and the slit width used was 1''. The median total signal-to-noise ratio (all wavelengths combined, ~ 3700 -6875 Å) was about 20 per pixel for foreground stars and GC candidates, with values ranging from 4 to over 100. If background galaxies, easily distinguished from these objects by their radial velocities, are included, the mean S/N per pixel is about 15.

Bias subtraction (with an averaged bias image), dark count correction, and flatfielding were done with IRAF's `ccdproc` task, and spectra were extracted using IRAF's `apall` task. Other tasks in the `specred` and `onedspec` packages were used to combine spectra, calibrate wavelengths, flux-calibrate the spectra using standard star observations taken each night, and eliminate pollutants such as cosmic rays and improperly-subtracted telluric lines.

Velocities were determined with the `xcsao` task in the `rvsao` package (Kurtz and Mink 1998) in IRAF using a list of standard SAO templates useful for the expected features of GCs, background galaxies, and foreground stars. Included are four templates derived from M31 GCs (`m31_a_temp`, `m31_f_temp`, `m31_k_temp`, and `fglotemp`), three galaxy absorption templates (`fm32temp`, `habtemp90`, and `fn4486btemp`), two composite stellar absorption templates (`fabtemp97` and `fallstars`), a synthetic HII region/galaxy emission template (`hemtemp0.0`), and a synthetic Ca H&K absorption template (`hkabstemp`). For each object, we list a heliocentric velocity determined from the template with the highest R value.

Objects labeled as clusters usually had spectra similar to G and early K giants. Mid-type K stars (\sim K3-K5) typically differed visibly from GC candidates in having a redder spectral energy distribution and strong Mg and Ca42 features. In order to provide a systematic, quantitative classification scheme to remove K dwarfs from the pool of GC candidates, we focused on the strong Ca42 feature and compared it to two other spectral features, G43 and H δ (using the H δ A index definition in Trager et al. (1998)). The difference between the Ca42 and H δ indices was used by Perelmuter, Brodie, and Huchra (1995) to distinguish between

K dwarfs and GC candidates. In our own samples, the Ca42 index also appeared strong in comparison to the G43 index in objects that had the spectral features of mid-K-type stars. To quantify the differences in these features between GCs and K dwarfs, we measured the Ca42, H δ A, and G43 indices in the 41 Schiavon et al. (2005) Milky Way GC spectra and in 16 K dwarfs from the Jones CoudéFeed spectral library described in Leitherer et al. (1996). The K dwarfs range in type from K0 to K8. Figure 2 shows histograms of Ca42-G43 and Ca42-H δ A ratios for the Milky Way GCs and Jones CoudéFeed K dwarfs respectively. There is some overlap between the distributions of Ca42-G43 for GCs and K dwarfs, particularly among early K-type stars (K0-K2), but this index appears useful for screening out mid-K-type stars in our sample. The Ca42-H δ A ratio seems more effective in discriminating between GCs and K dwarfs, with the only K dwarf overlapping the MW GC range of values being a K8 star, which in our NGC 300 sample would be easily distinguishable from a GC. The Milky Way GCs had a mean Ca42-G43 value of -0.057 with a σ of 0.024 and a mean Ca42-H δ A value of 0.016 with a σ of 0.075.

For an object to be considered a GC candidate, we insisted that it have both Ca42-G43 ≤ 0.05 (the value for NGC 300-05 which, despite having a Ca42-G43 ratio more than 3σ above the MW GCs, has been visually confirmed as a GC via HST archive images) and Ca42-H δ A ≤ 0.241 (3σ above the Milky Way GC mean). This analysis excludes NGC 300cr and NGC 300df on the basis of Ca42-H δ A but not Ca42-G43 (which one might expect for K0-K2 dwarfs), and NGC 300ax, previously classified by Olsen et al. (2004) as a GC, on the basis of Ca42-G43 but not Ca42-H δ .

Radial velocity can provide limited additional information on the likelihood of an object being a star or a GC. Since the heliocentric radial velocity of NGC 300 is fairly low — $+142 \pm 4 \text{ km s}^{-1}$ (de Vaucouleurs et al. 1991) — it is impossible to eliminate all stars and keep all GCs in the sample if a strict velocity cut is used to exclude candidates. Hence, we cannot automatically label objects with clusterlike spectra but very low radial velocities as definite stars. The velocity dispersion in NGC 300’s halo is estimated by Carignan and Freeman (1985) to be 60 km s^{-1} . If the Milky Way halo were non-rotating, the average expected radial velocity of a Galactic star in the direction of NGC 300 would be about $+40 \text{ km s}^{-1}$, and the velocity dispersion of the Milky Way halo is about 130 km s^{-1} (as viewed from the center of the Milky Way). So while there’s a 95% chance that an NGC 300 halo object will have a radial velocity greater than 20 km s^{-1} , Milky Way halo stars can very easily have velocities similar to those of genuine NGC 300 GCs. This means that most objects with negative radial velocities will be Milky Way stars, but those with positive radial velocities could easily be either foreground stars or NGC 300 clusters, and only spectral features or high-resolution imaging can distinguish them. On the basis of radial velocity, we flag three objects with spectral features similar to GC candidates - NGC 300cm, NGC 300co, and NGC

300db - as possible stars. All have radial velocities less than 0 km s^{-1} .

Figure 3 shows the correlations between our two indicators of star vs. GC status, Ca42-G43 and Ca42-H δ A, and the radial velocities of foreground stars and GC candidates in NGC 300. Both trends are high in scatter, demonstrating the difficulty in measuring star vs. GC status on the basis of radial velocity. The correlation between Ca42-H δ A and radial velocity is somewhat stronger, probably due to its greater sensitivity to K0-K2 dwarfs compared to Ca42-G43.

The best-fit velocity template also hints at whether an object is likely to be a star or a cluster. The templates we used included several templates developed using intermediate-age and old stellar populations (m31_a_temp, m31_f_temp, m31_k_temp, fglotemp, and fm32temp), a couple templates suited for field stars (fallstars, fabtemp97), and a couple synthetic templates (hemtemp0.0 for HII emission and hkabstemp for Ca II H & K absorption). Most GCs were best fit by the M31 F and K templates, while many foreground dwarfs were best fit by the stellar absorption templates.

Figure 4 shows sample spectra of an old GC, a typical foreground K star, and a background galaxy. The region shown in the plot covers wavelengths from 3700 to 5300Å, containing key features such as CNB, CaI 4227, G4300, H β , Mgb, and several Fe features. One can see the K star’s strong CaI 4227 and Mgb features, compared to the relatively weak CaI 4227 and Mgb and strong G4300 of the GC. One can also see that in the foreground star, the continuum on the blue side of the Mg2 feature tends to be notably fainter than on the red side. The galaxy is recognizable by its visibly redshifted CaII H&K lines.

3. Discovering Clusters

The names, heliocentric cross-correlation velocities, and object types (background galaxy, foreground star, cluster candidate) are shown in Table 1. The objects with number designations 1-17 are from Kim et al. 2002; the rest are from Olsen et al. 2004. Of the 17 Kim et al. candidates, only five — objects 2, 3, 4, 5, and 12 — appear to be old GCs. Note that object 3 is also NGC 300a in Olsen et al.’s catalog, and has been proven a GC and spectroscopically evaluated by Olsen and collaborators. Most of the remaining Kim et al. objects were background galaxies, except for one HII region (Object 6) and three probable NGC 300 stars (NGC 300-09, M-type; NGC 300-10, F-type; and NGC 300-15, A-type).

Since GCs in NGC 300 can easily be resolved with HST, we searched the HST ACS and WFPC2 archives for images of our NGC 300 objects. The images were from programs GO-8584, GO-9162, GO-9492, and GO-10915. We found eight Kim et al. objects in the

archival HST images: Objects 1, 5, 6, 7, 8, 9, 10, and 11. These eight objects, imaged in F555W for the ACS images of Objects 1, 5, 6, 7, and 11 and F606W for the WFPC2 images of Objects 8, 9, and 10, are shown in Figure 5. Generally, their appearances match what we expect based on their spectra. Objects 1, 7, and 11 are spiral galaxies; Object 8 is an early-type galaxy; Object 6 is an HII complex; Object 5 appears to be a genuine GC; and Objects 9 and 10, initially considered as possible open clusters, appear pointlike but non-saturated and without diffraction spikes. Their Kim et al. (2002) V magnitudes are 19.73 for NGC 300-09 (which has an M-type spectrum) and 19.12 for NGC 300-10 (which has an F-type spectrum), consistent with supergiant stars in NGC 300. They both have many fainter stars surrounding them, so may also be open clusters or stellar blends.

Kim et al. selected their GC candidates by using a color cut ($0.3 < B - V < 2.0$) and morphological considerations, including visual inspection of the shapes and brightness profiles. They assigned three “classes” to the quality of GC candidates, Class 1 being most likely to be GCs and Class 3 being least likely. Interestingly, Class 2 yielded the highest fraction of objects that turned out to be GCs: 3 out of 7 had GC spectra, as compared to 1 out of 4 for Class 1 and 1 out of 6 for Class 3. Kim et al. reported using morphological considerations to determine the probability of an object being a GC. If they required that the clusters be resolved from the ground to be Class I objects, they may have actually shifted the balance out of favor of true GCs and in favor of galaxies, since a typical GC at the distance of NGC 300 is close to $1''$ in diameter, which is the limit imposed by typical ground-based seeing.

Of the Olsen et al. candidates, 11 objects appeared to be stars, including NGC 300ax, which Olsen et al. had identified and analyzed as a GC. Its spectrum has wide spectral lines consistent with a dwarf of late K to early M type: a wide but shallow Mgb (5180 \AA) feature and a wide and deep NaD (5895 \AA) feature, as well as having a strong CaI 4227 feature as compared to the G4300 feature much like other K dwarfs. In addition to this, 3 more GC candidates with $\text{Ca42-G43} \leq 0.05$ and $\text{Ca42-H}\delta\text{A} \leq 0.241$ have been flagged as possible stars on the basis of radial velocities less than 0 km s^{-1} .

4. Velocity Dispersion, Rotation, and Estimated Mass

Our GC velocities — 9 highly probable clusters and 3 low-velocity possible clusters — can be combined with seven previously observed GC velocities, five from Olsen et al. (2004) and two from unpublished data contributed by one of us (K. Olsen), to obtain a GC velocity dispersion and simple mass estimate for NGC 300. The velocities of the seven previously observed clusters are listed in Table 2. Figure 6 shows the velocity histogram of all GC

candidates, both previously observed by Olsen et al. and observed in this paper, including those with $V < 0$.

If we include all highly probable and possible cluster candidates — 19 objects in all — we have a mean velocity of 79 km s^{-1} and a velocity dispersion, corrected for the mean uncertainty of the velocities, of 92 km s^{-1} . If we exclude the three $V < 0$ objects, we have 16 objects with a mean velocity of 107 km s^{-1} and an uncertainty-corrected velocity dispersion of 68 km s^{-1} . This latter dispersion is closer to the Carignan and Freeman (1985) theoretical velocity dispersion estimate of 60 km s^{-1} than is the velocity dispersion of all 19 objects.

We can also investigate whether there is evidence for rotation among our GCs. Figure 7 shows the velocity of cluster candidates as a function of position angle, along with a fit to the rotation of all candidates not labeled as possible stars and a representation of the Puche, Carignan, and Bosma (1990) HI rotation curve (with the velocity of 90 km s^{-1} reduced by a factor of $\sin(i)$ with $i = 42.3^\circ$). We fit a function of the form

$$V(\theta) = V_c + V_{pr} * \sin(\theta - \theta_0) \quad (1)$$

to the velocities and position angles of the 16 cluster candidates with $V > 0$, presumed to be the best cluster candidates. V_c is the central velocity, V_{pr} is the projected rotational velocity (the actual rotational velocity times $\sin(i)$), θ is the position angle of the cluster in degrees measured east from north, and θ_0 is the position angle of the rotation axis. Using a nonlinear least-squares fit with weights equal to $1/\sigma_v^2$, fitted to all $V < 0$ clusters, we found $V_c = (122 \pm 21) \text{ km s}^{-1}$, $V_{pr} = (91 \pm 32) \text{ km s}^{-1}$, and $\theta_0 = (27^\circ \pm 17^\circ)$. However, this rotation curve seems exceptionally strong and out of phase with the HI rotation, and the uncertainty-corrected dispersion of the GC velocities minus their predicted rotational velocities is actually considerably worse than our previous result (80 km s^{-1}). An unweighted fit to the same points gives a similarly unsatisfactory result: $V_c = 122 \pm 22 \text{ km s}^{-1}$, $V_{pr} = (42 \pm 34) \text{ km s}^{-1}$, and $\theta_0 = (164^\circ \pm 35^\circ)$, and still a worse velocity dispersion than without rotation (81 km s^{-1}). We therefore conclude that there is no sign of rotation in our GC sample.

We use the Projected Mass Estimator (Heisler, Tremaine, and Bahcall 1985) to estimate the total mass of NGC 300, both using the means of the total and “good” samples and the mean velocity of NGC 300 itself. The equation for the projected mass estimator is as follows:

$$M_{PM} = \frac{f_{pm}}{G(N - \alpha)} \sum_i V_{zi}^2 R_{\perp i} \quad (2)$$

Here we use $f_{pm} = 32/\pi$ (for isotropic orbits, recommended by Heisler, Tremaine, and Bahcall (1985) and $\alpha = 1.5$. Using the published mean velocity of NGC 300 itself gives $M_{PM} = (1.8 \pm 0.8) \times 10^{11} M_\odot$ for the total sample, and $M_{PM} = (8.3 \pm 2.1) \times 10^{10} M_\odot$ for the $V > 0$

subsample. The total sample reaches a maximum projected radius of 12.1 kpc, and the $V>0$ sample reaches a maximum of 11.6 kpc. Uncertainties were estimated using the bootstrap method with 1000 resamplings. Puche, Carignan, and Bosma (1990), using HI rotation curve data, calculate a mass of $2.4 \times 10^{10} M_{\odot}$ out to 10.6 kpc; Rhee and Chun (1992) give mass-model-based estimates for the mass of NGC 300 ranging from $2.8 - 4.2 \times 10^{10} M_{\odot}$. Overall, our masses run large but are not outside the realm of possibility.

5. Metallicity Analysis

We measured 26 spectral indices, including the 12 indices calibrated in Brodie and Huchra (1990) using the Brodie and Huchra (1990) bandpass definitions and the diagnostic $H\delta A$ index with the Trager et al. (1998) bandpass definition. Eight of the Brodie and Huchra indices are mostly similar to the Lick/IDS bandpass definitions, differing slightly from those of Worthey et al. (1994) and Trager et al. (1998). All spectral indices not in Brodie and Huchra (1990) were measured using the bandpass definitions of Trager et al. (1998). All bandpasses were shifted to the uncorrected, geocentric radial velocities of our objects. Our indices are not true Lick indices because our spectra have not been degraded to match the resolution of the Lick star spectra, and we did not observe any Lick standard stars to calibrate the fluxes and indices precisely. However, we did observe a template galaxy (NGC 1052) that was also observed by Brodie and Huchra (1990), and found the overlapping indices to be similar to theirs. All indices are given in magnitudes, as in Brodie and Huchra, for easy comparison with their M31 spectral indices and index-metallicity calibration methods. Converting to equivalent width requires multiplication by the bandwidth of the central index band shifted to the object’s velocity.

We determined metallicities using a method based on the Brodie and Huchra (1990) prescription, but with new index-vs.-metallicity calibrations determined from the 41 Milky Way spectra from Schiavon et al. (2005), degraded to match the 5 \AA resolution of our spectra. We determined linear regressions for metallicity (from Harris (1996) for each Milky Way GC) as a function of index strength for all our indices, as well as the “range” R_I defined as in Brodie and Huchra (1990), and the σ_m representing the scatter about the regression line. We used the R_I and σ_m values to construct weights similar to those in Brodie and Huchra (1990):

$$W_I = \frac{R_I}{(\sigma_m^2 + \sigma_p^2 + \sigma_s^2)^{1/2}} \quad (3)$$

with σ_p being the photometric uncertainty in the entire index, the quadrature sum of the uncertainties in each band. To calculate σ_s , the measure of our ability to measure the same index repeatedly for the same object over the course of different nights and conditions, we

used spectral index measurements for the standard star LTT 9239, which we observed each night. We modified the formula for the uncertainty in a band (continuum or feature value for an index) from Brodie and Huchra (1990) to the following:

$$snr = 1/\sigma_B = O/(O + S + R^2)^{1/2}, \quad (4)$$

where O is the number of object counts per pixel, S is the number of sky counts per pixel, and R is the read noise. The weighted average and uncertainty in the weighted average were determined as in Brodie and Huchra (1990).

Our choice of indices to use in the weighted average was determined by considering the correlation coefficient in each Milky Way linear fit, the signal-to-noise ratio in the NGC 300 objects, and the degree of scatter in NGC 300 index-index relations. The final set of indices - Mg2, Fe5270, Fe5335, Ca4227, G4300, δ , Ca4455, and CN2 - all had relatively high correlation coefficients in the Milky Way index-metallicity relations and relatively high signal-to-noise in typical NGC 300 clusters.

Table 3 lists measurements and uncertainties of the 12 indices calibrated in Brodie and Huchra and the H δ A index used to help screen out foreground stars, and Table 4 gives the measurements and uncertainties of the remaining 13 indices. Table 5 lists the linear relationships between index and metallicity for the 8 indices we chose along with σ_s measurements based on the standard star LTT 9239, and Table 6 lists derived metallicities for our clusters, along with five spectroscopically determined metallicities for Sculptor Group GCs from Olsen et al. (2004). The highest σ_s for spectral features used to measure metallicity was 0.095 (the δ index, in the region with the lowest signal-to-noise ratio and spanning a broad range of wavelengths) and the lowest was 0.001 (Fe5270, a narrow feature in the region with the highest signal-to-noise ratio).

Figures 8-12 compare various spectral indices to those of Andromeda Galaxy GCs (Huchra, Brodie, and Kent 1991; Barmby et al. 2000) and the Schiavon et al. Milky Way GCs. Figure 8 shows that the CNR index lies below typical values for Andromeda and Milky Way clusters, while the CNB index, traditionally considered a more reliable indicator of actual CN content, looks about the same as the other galaxies. Figure 9 shows a close-up of the CNB region for averages of 10 Milky Way GCs and 10 NGC 300 GCs matched for Fe52 strength. The CNB depths look fairly similar, although a tilt due to the high reddening of many of the MW GCs is visible. Fe52 metallicities, as seen in Figure 10, look similar in all three galaxies. The G-band (Figure 11) seems about 0.02 mag high compared to the Milky Way and Andromeda, although overall more similar to the Milky Way. And finally, H β , the index that is sensitive to age and inversely correlated with metallicity, is shown in Figure 12. NGC 300 GCs show a mean and distribution more similar to the Milky Way than to Andromeda, suggesting old clusters similar to those of the Milky Way.

The deficit in CNR in our sample does not necessarily indicate a nitrogen deficiency in the GCs of NGC 300, especially given the apparently normal CNB. Andromeda GCs had once been thought to have nitrogen excesses compared to Milky Way GCs (Burstein et al. 1984; Brodie and Huchra 1991), but this was later challenged when the metal-rich Milky Way GCs were taken into account (Puzia et al. 2002). Instead, Puzia et al. found that metal-rich GCs in both Andromeda and the Milky Way were nitrogen-enhanced compared to the general old stellar populations of galaxies, which they propose may be due to low-mass GC stars accreting carbon and/or nitrogen from the AGB winds of dying higher-mass stars in the cluster. A deficiency in CNR in our sample, therefore, may suggest a high rate of foreground star contamination especially among metal-rich objects, since stars should lack nitrogen compared to metal-rich GCs of similar metallicity. However, CNB is normal, and CNR is a weak feature that can easily be trumped by noise, so there may not be any cause for alarm. Two of the four objects on the lower right of the CNR vs. Mg2 plot (Figure 8(b)), with Mg2 indices above +0.125 and lacking strong CNR, are among the low-velocity candidates.

Overall, the NGC 300 GCs seem similar to those of the Milky Way.

Figure 13 shows the metallicity distribution of the NGC 300 GCs as compared to the Milky Way, Andromeda, and M33, including NGC 300r from Olsen et al. (2004). With all candidates included, the distribution appears unimodal and rather metal-rich. With the three low-velocity objects excluded, the distribution appears to still be fairly metal-rich. The NGC 300 cluster sample is too small and possibly too contaminated to definitively determine bimodality or a lack thereof.

An updated version of the Brodie and Huchra (1991) relation between mean GCS metallicity and total galaxy luminosity was created using relatively recent published galaxy distance and spectroscopic GC metallicity information from the literature on several galaxies, along with contemporary 2MASS K and de Vaucouleurs et al. (1991) B magnitudes found on the NASA/IPAC Extragalactic Database (NED). Table 7 summarizes the data, gathered from a wide variety of studies of GCSs using different selection criteria. The relationship between the mean GCS metallicity and absolute B magnitude is shown in Figure 14, and the relationship between mean GCS metallicity and absolute 2MASS K magnitude is shown in Figure 15. NGC 300, with its calculated mean GC metallicity of -0.94 ± 0.15 , lies above both the early-type and late-type galaxies on the plot. The high metallicity calculated for NGC 300 could be due to most of the “higher metallicity” cluster candidates being foreground stars, as suggested above in the discussion of CNR weakness. If the three clusters deemed to be possible foreground stars are eliminated, the mean metallicity of the remaining ten clusters (our clusters plus NGC 300r) is -0.98 ± 0.12 , which is still higher than expected

for a galaxy the size of NGC 300. Besides possible foreground star contamination, color selection in the candidate samples may have created a bias in favor of metal-rich, intrinsically red clusters that drastically increases their relative numbers in our tiny sample. This is unlikely for the Kim et al. clusters, but the Olsen et al. (2004) color cuts were found to be ~ 0.2 mag redder than initially thought due to a calibration error. It is also worth noting that the spectroscopic metallicity estimates used in our metallicity-luminosity relations do not distinguish among the $[\alpha/Fe]$ values that may differ among galaxy types.

6. Summary/Conclusions

The GCS of NGC 300 appears to have features similar to that of the Milky Way. Its place on the metallicity-luminosity relation is consistent with the positive correlation between galaxy luminosity and mean GC metallicity, although the average metallicity of our NGC 300 cluster sample is higher than expected. Eliminating all ambiguous objects from our cluster sample gives a mean metallicity slightly more consistent with the Milky Way and Andromeda. The GCs, excluding those deemed possible stars, have a velocity dispersion of 68 km s^{-1} , and may be rotating, although the evidence does not strongly favor rotation. The high mean metallicity of our cluster sample may be primarily a result of the difficulty in screening out stars without the ability to use radial velocity cuts. The problem of mistaking foreground stars (and giant stars within the target galaxy) for GCs could easily be remedied with more space-based imaging of NGC 300. GCs could then be identified visually or with more accurate size and shape determinations before spectroscopic study.

We would like to thank the LCO staff for helping us use the Magellan Telescopes and instruments. This work has been supported by the Smithsonian Institution and Harvard College Observatory. We also thank Ricardo Schiavon and collaborators for making their Milky Way spectra available to the public at <http://www.noao.edu/ggclib/>.

REFERENCES

- Ashman, K. M., and Zepf, S. E. 1992, *ApJ*, 384, 50.
- Barmby, P., Huchra, J. P., Brodie, J. P., Forbes, D. A., Schroder, L. L., and Grillmair, C. J., 2000, *AJ*, 119, 727.
- Beasley, M. A., Bridges, T., Peng, E., Harris, W. E., Harris, G. L. H., Forbes, D. A., Mackie, G. 2008, *MNRAS*, 386, 1443.

- Beasley, M. A., Forbes, D. A., Brodie, J. P., and Kissler-Patig, M. 2004, *MNRAS*, 347, 1150.
- Bersier, D. 2000, *ApJ*, 543, L23.
- Brodie, J. P., and Huchra, J. P. 1990, *ApJ*, 362, 503.
- Brodie, J. P., and Huchra, J. P. 1991, *ApJ*, 379, 157.
- Brodie, J. P., and Strader, J. 2006, *ARA&A*, 44, 193.
- Burstein, D., Faber, S., Gaskell, M., and Krumm, N. 1984, *ApJ*, 287, 586.
- Cappellari, M. et al. 2006, *MNRAS*, 366, 1126.
- Carignan, C. and Freeman, K. C. 1985, *ApJ*, 294, 494.
- Chandar, R., Whitmore, B., and Lee, M. G. 2004, *ApJ*, 611, 220.
- Chomiuk, L., Strader, J., and Brodie, J. 2008, *AJ*, 136, 234.
- Cohen, J. G., Blakeslee, J. P., and Côté, P. 2003, *ApJ*, 592, 866.
- Côté, P., Marzke, R. O., and West, M. J. 1998, *ApJ*, 501, 554.
- de Vaucouleurs, G., de Vaucouleurs, A., Corwin Jr., H. G., Buta, R. J., Paturel, G., and Fouqué, P. 1991, *Third Reference Catalog of Bright Galaxies, Version 3.9* (New York: Springer-Verlag)
- Ferrarese, L. et al. 2000, *ApJ*, 529, 745.
- Forbes, D. A., Brodie, J. P., and Grillmair, C. J. 1997, *AJ*, 113, 1652
- Freedman, W. 1990, *ApJ*, 355, L35
- Freedman, W. L., Hughes, S. M., Madore, B. F., Mould, J. R., Lee, M. G., Stetson, P., Kennicutt, R. C., Turner, A., Ferrarese, L., Ford, H., Graham, J. A., Hill, R., Hoessel, J. G., Huchra, J., and Illingworth, G. D. 1994, *ApJ*, 427, 628.
- Galleti, S., Bellazzini, M., and Ferraro, F. R. 2004, *A&A*, 423, 925.
- Gieren, W., Pietrzyński, G., Walker, A., Bresolin, F., Minniti, D., Kudritzki, R., Udalski, A., Sosziński, I., Fouqué, P., Storm, J., and Bono, G. 2004, *AJ*, 128, 1167.
- Harris, W. E. 1996, *AJ*, 112, 1487.
- Heisler, J., Tremaine, S., and Bachall, J. N. 1985, *ApJ*, 298, 8.

- Huchra, J. P., Brodie, J. P., and Kent, S. M. 1991, *ApJ*, 370, 495.
- Jarrett, T. H., Chester, T., Cutri, R., Schneider, S. E., and Huchra, J. P. 2003, *AJ*, 125, 525.
- Jensen, J. B., Tonry, J. L., Barris, B. J., Thompson, R. I., Liu, M. C., Rieke, M. J., Ajhar, E. A., and Blakeslee, J. P. 2003, *ApJ*, 583, 712.
- Kang, A., Kim, J., Shin, I., Chun, S., Kim, H., and Sohn, Y. 2007, *JASS*, 24, 203.
- Kim, S.C., Sung, H., and Lee, M.G. 2002, *JKAS*, 35, 9.
- Kissler-Patig, M., Brodie, J. P., Schroder, L. L., Forbes, D. A., Grillmair, C. J., and Huchra, J. P. 1998, *AJ*, 115, 105.
- Kundu, A. and Whitmore, B. C. 1998, *AJ*, 116, 2841.
- Kurtz, M. J. and Mink, D. J. 1998, *PASP*, 110, 934.
- Larsen, S. S. and Brodie, J. P. 2002, *AJ*, 123, 1488.
- Larsen, S. S., Brodie, J. P., Beasley, M. A., and Forbes, D. A. 2002, *AJ*, 124, 828.
- Larsen, S. S., Brodie, J. P., Huchra, J. P., Forbes, D. A., and Grillmair, C. J. 2001, *AJ*, 121, 2974.
- Lee, M. G., Kim, E., and Geisler, D. 1998, *AJ*, 115, 947.
- Leitherer, C. et al. 1996, *PASP*, 108, 996.
- McConnachie A.W., Irwin M.J., Lewis G.F., Ibata, R.A., Chapman, S.C. Ferguson A.M.N., Tanvir N., 2004, *MNRAS*, 351, L9
- Nantais, J. B., Huchra, J. P., Barmby, P., Olsen, K. A. G., and Jerret, T. H. 2006, *AJ*, 131, 1416.
- Norris, M. A., Sharples, R. M., Bridges, T., Gebhart, K., Forbes, D. A., Proctor, R., Raul Faifer, F., Carlos Forte, J., Beasley, M. A., Zepf, S. E., and Hanes, D. A. 2008, *MNRAS*, 385, 40.
- Olsen, K. A. G., Miller, B. W., Suntzeff, N. B., Schommer, R. A., and Bright, J. 2004, *AJ*, 127, 2674.
- Perelmuter, J., Brodie, J. P., and Huchra, J. P. 1995, *AJ*, 110, 620.
- Proctor, R. N., Forbes, D. A., Brodie, J. P., and Strader, J. 2008, *MNRAS*, 385, 1709.

- Puche, D., Carignan, C., and Bosma, A. 1990, *AJ*, 100, 1468.
- Puzia, T. H., Saglia, R. P., Kissler-Patig, M., Maraston, C., Greggio, L., Renzini, A., and Ortolani, S. 2002, *A&A*, 395, 45.
- Rejkuba, M. 2004, *A&A*, 413, 903.
- Rhee, M. and Chun, M. 1992, *JKAS*, 25, 11.
- Schiavon, R. P., Rose, J. A., Courteau, S., and MacArthur, L.A. 2005, *ApJS*, 160, 163.
- Schröder, L. L., Brodie, J. P., Kissler-Patig, M., Huchra, J. P., and Phillips, A. C. 2002, *AJ*, 123, 2473.
- Sharina, M. E., Afanasiev, V. L., and Puzia, T. H. 2006, *MNRAS*, 372, 1259.
- Sikkema, G., Peletier, R. F., Carter, D., Valentijn, E. A., and Balcells, M. 2006, *A&A*, 458, 53.
- Strader, J., Brodie, J. P., and Forbes, D. A. 2004, *AJ*, 127, 295.
- Strader, J., Brodie, J. P., Forbes, D. A., Beasley, M. A., and Huchra, J. P. 2003, *AJ*, 125, 1291.
- Tonry J.L., Dressler A., Blakeslee J.P., Ajhar E. A., Fletcher A.B., Luppino G.A., Metzger M.R., and Moore C.B. 2001, *ApJ*, 546, 681.
- Trager, S. C., Worthey, G., Faber, S. M., Burstein, D., and Gonzalez, J. J. 1998, *ApJS*, 116, 1.
- Worthey, G., Faber, S., Gonzalez, J. J., and Burstein, D. 1994, *ApJS*, 94, 687.
- Zinn, R. 1985, *ApJ*, 283, 424.

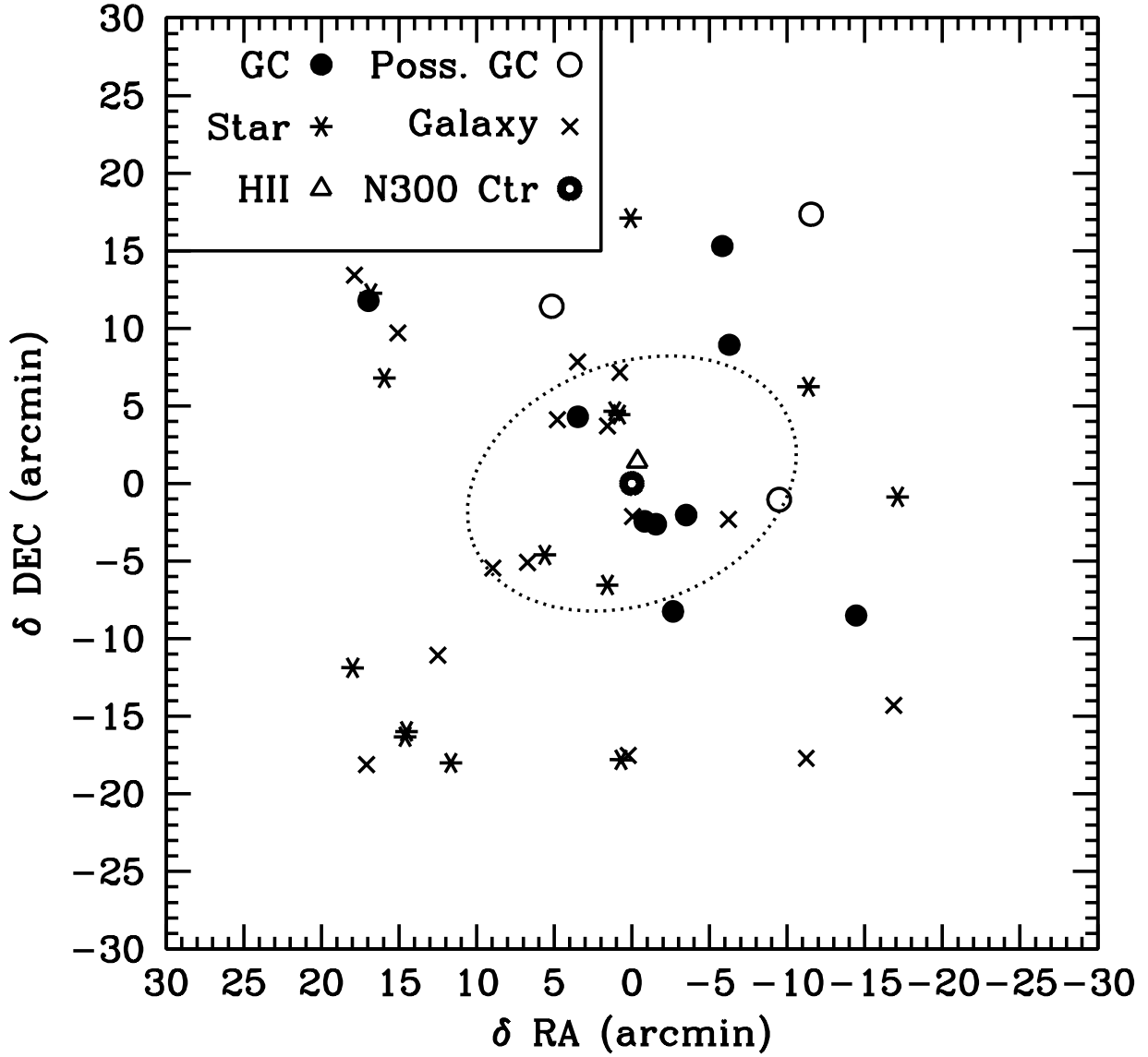


Fig. 1.— Locations of various objects in NGC 300, including GCs, “possible” GCs (low velocity candidates), galaxies, stars, and HII regions. The dotted line represents the disk of NGC 300.

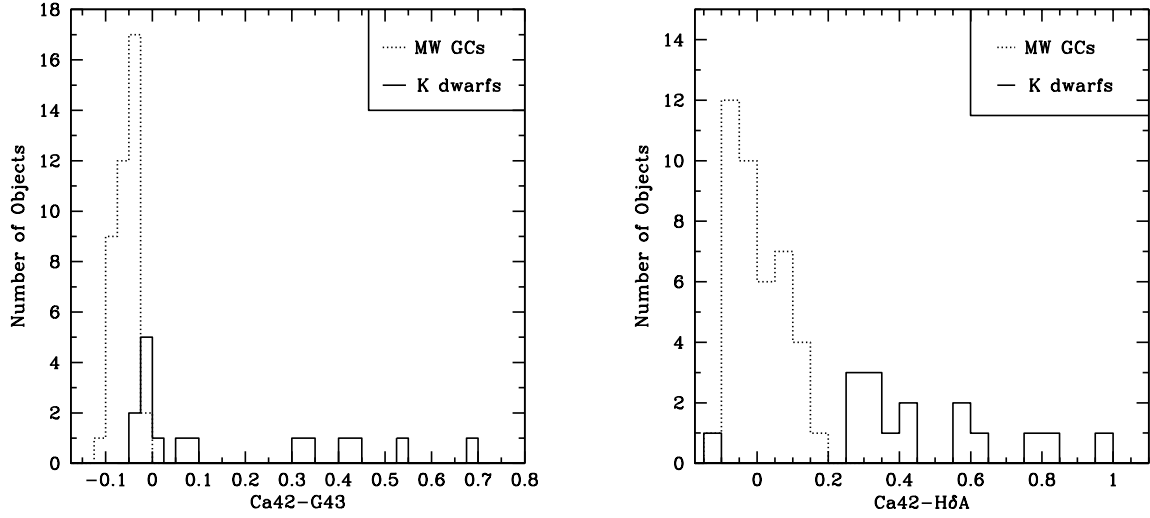


Fig. 2.— Histograms of Ca42-H δ A and Ca42-G43 index ratios for Milky Way GCs and Milky Way field K stars.

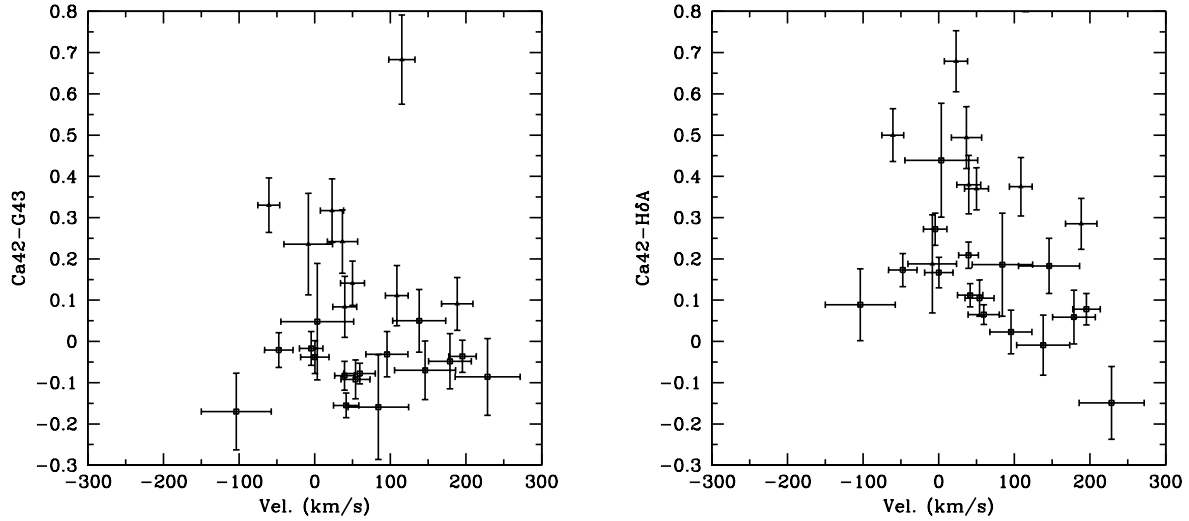


Fig. 3.— Ca42-G43 (left) and Ca42-H δ A (right) vs. radial velocity for all low-radial-velocity objects (foreground stars and GC candidates).

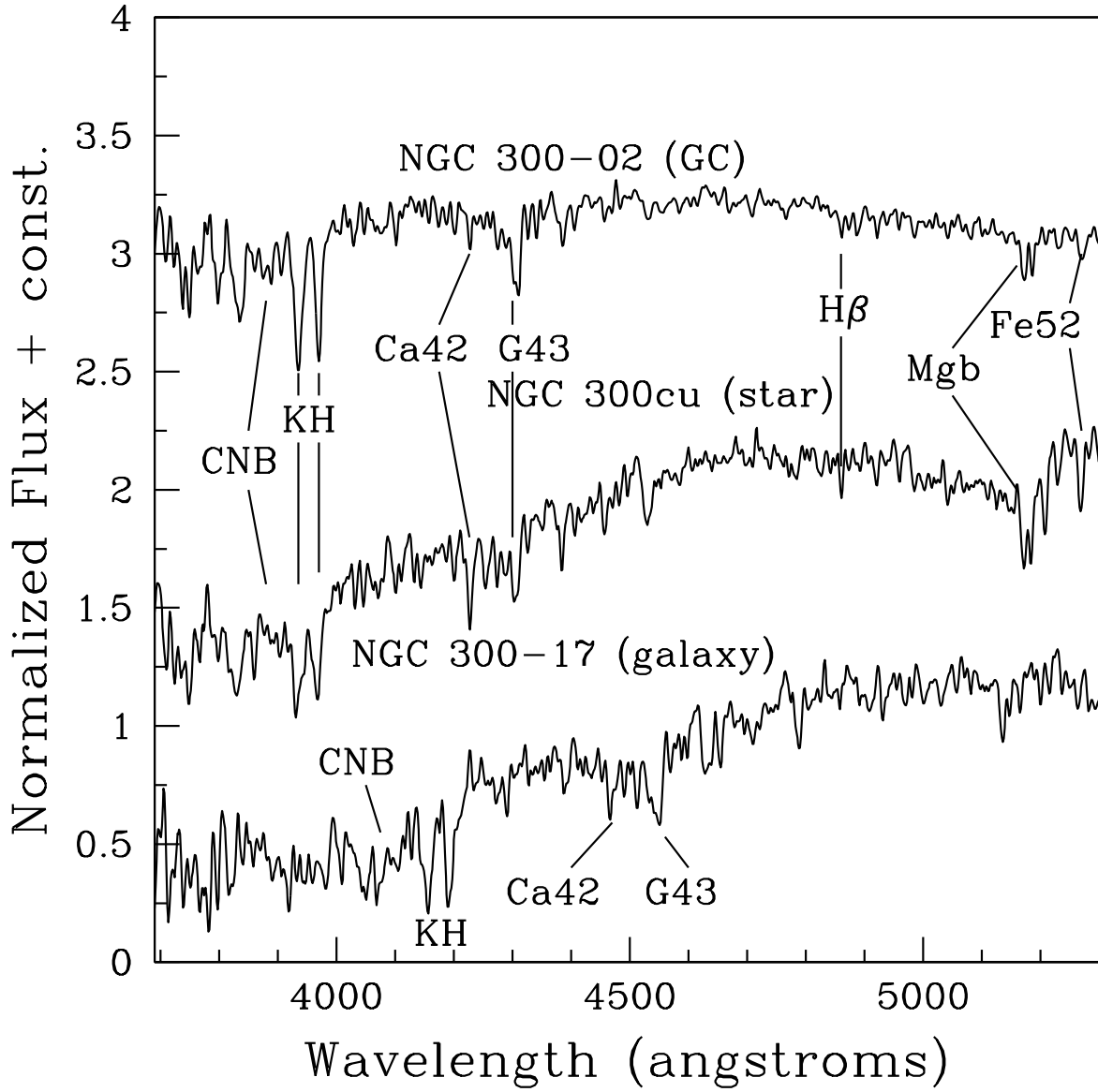


Fig. 4.— Sample spectra of a GC (top), a foreground star (middle), and a background galaxy (bottom), normalized and shown on the same scale.

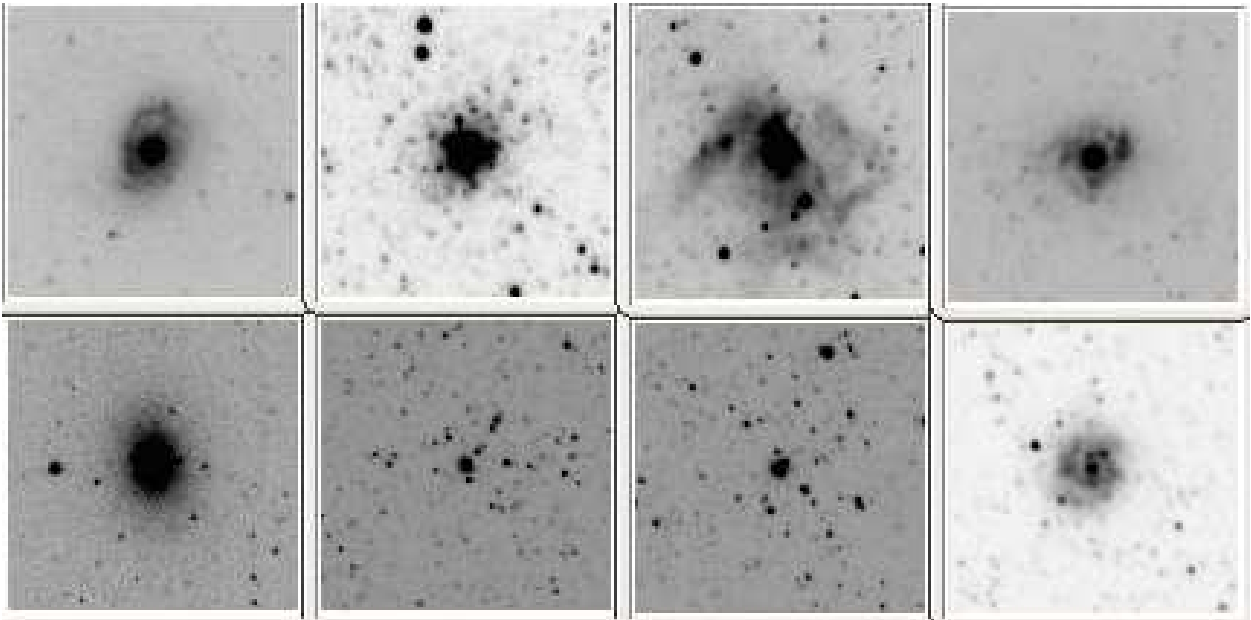


Fig. 5.— NGC 300 objects from the Kim et al. catalog found in the HST archives. On the top row, left to right, are Kim et al. Objects 1, 5, 6, and 7; on the bottom row, left to right, are Kim et al. objects 8, 9, 10, and 11. Objects 1, 5, 6, 7, and 11 are imaged in F555W by ACS/WFC and Objects 8, 9, and 10 are imaged in F606W by WFPC2.

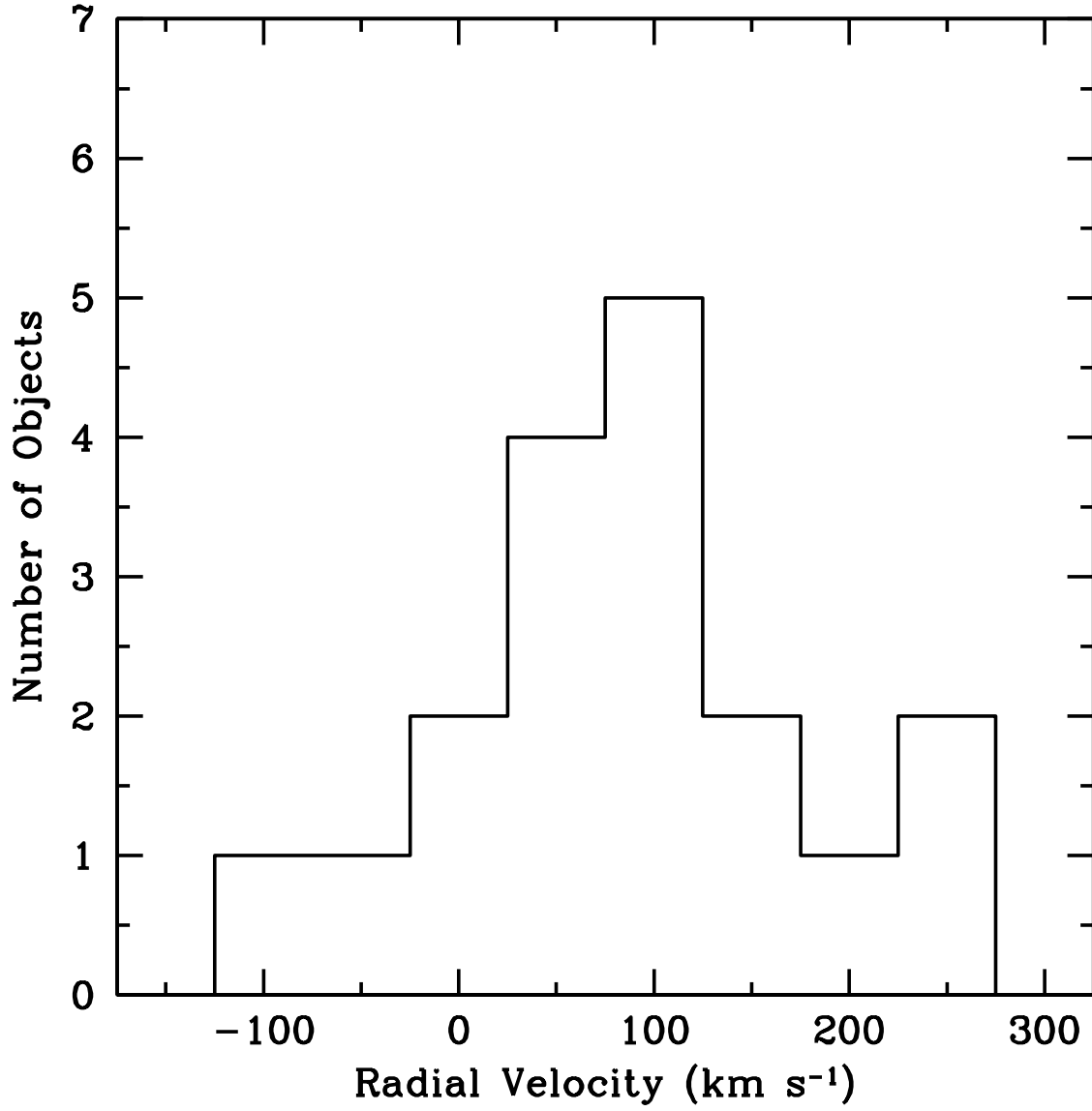


Fig. 6.— Velocity histogram of all NGC 300 GC candidates, including those confirmed by Olsen et al.

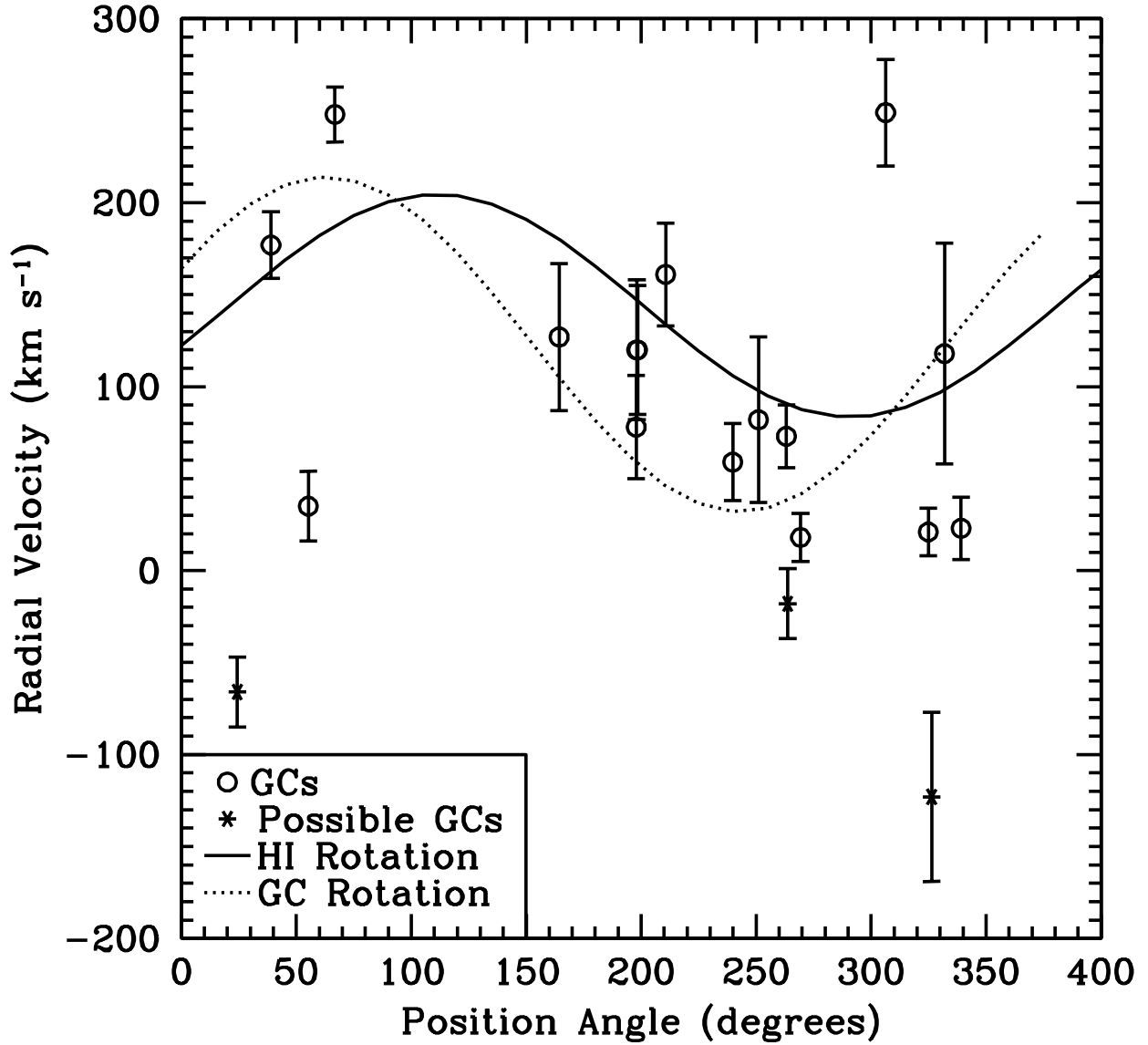


Fig. 7.— Velocity vs. position angle for the 14 highly probable GCs (open circles) and 3 possible GCs (stars), shown with a representation of the HI rotation curve (solid line) and a rotation curve calculated for the 14 highly probable GCs (dotted line).

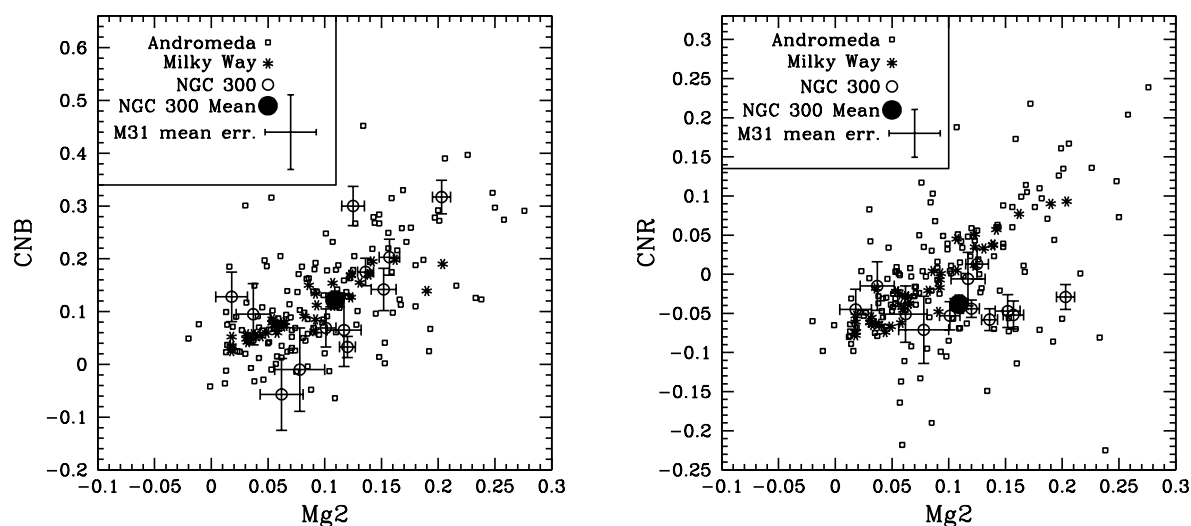


Fig. 8.— CN indices (blue on left, red on right) vs. Mg2 index. Open squares represent Andromeda clusters, asterisks represent Milky Way clusters, and open circles represent Sculptor Group clusters. A large filled circle marks the mean of the NGC 300 clusters. The average error bar for M31 is shown in the legend. The average Milky Way uncertainty was smaller than the size of the symbols and therefore omitted.

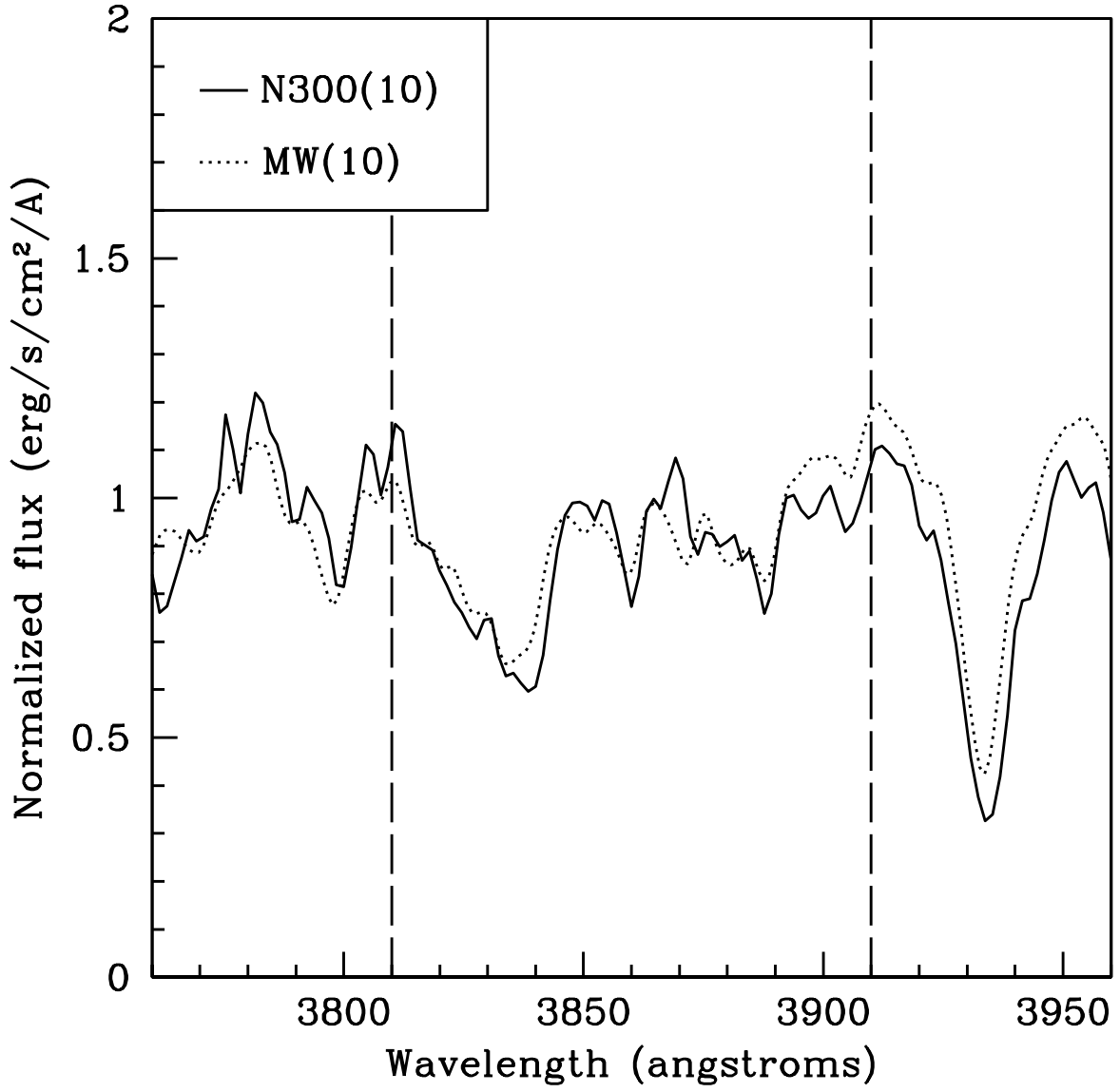


Fig. 9.— CNB feature for averages of 10 NGC 300 GCs and 10 MW GCs matched for Fe52 index strength.

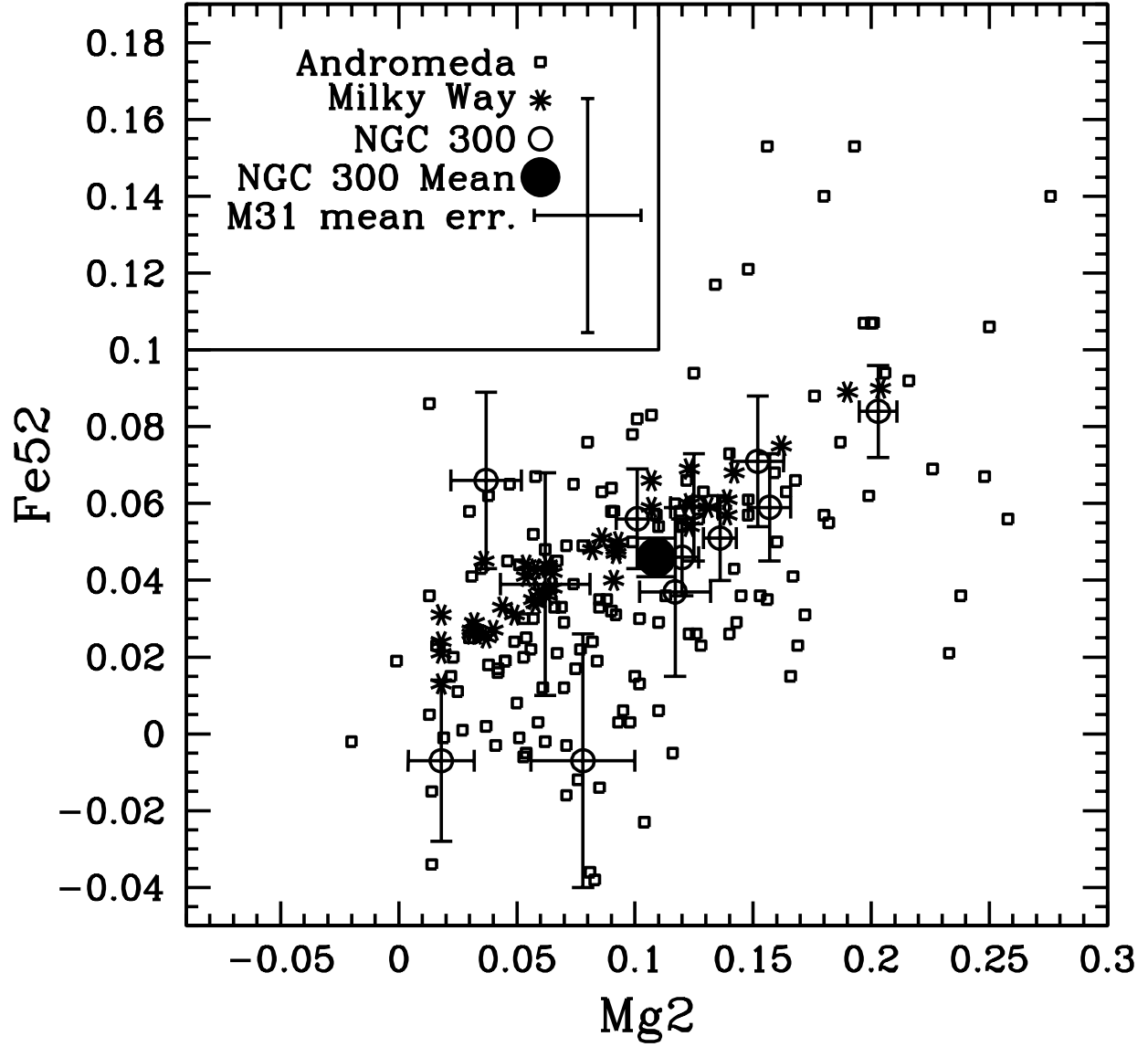


Fig. 10.— Fe-5270 index vs. Mg2 index. Symbols are the same as in Figure 4.

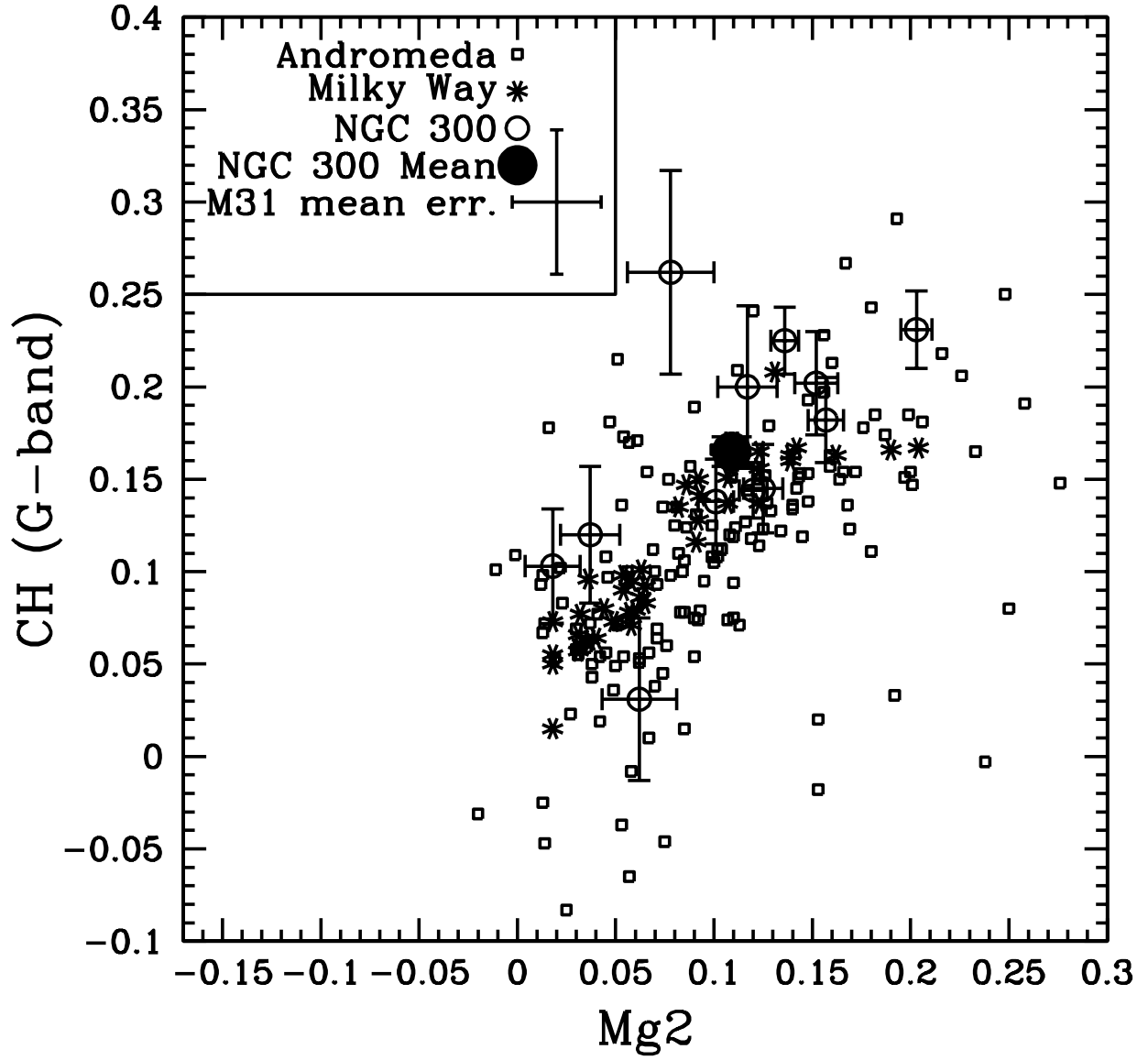


Fig. 11.— G-band (CH) index vs. Mg2 index. Symbols are the same as in Figure 4.

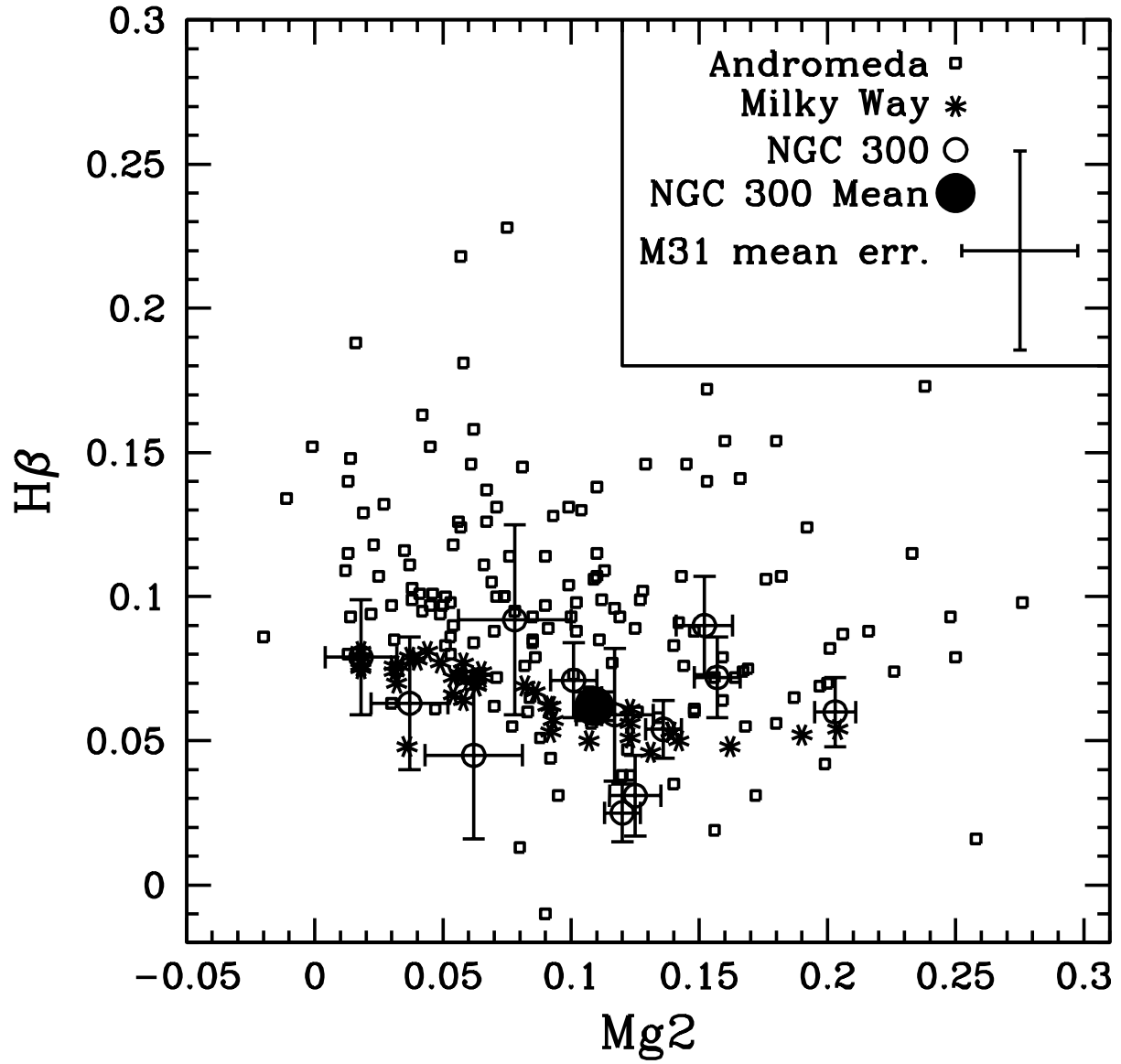


Fig. 12.— H β index vs. Mg2 index. Symbols are the same as in Figure 4.

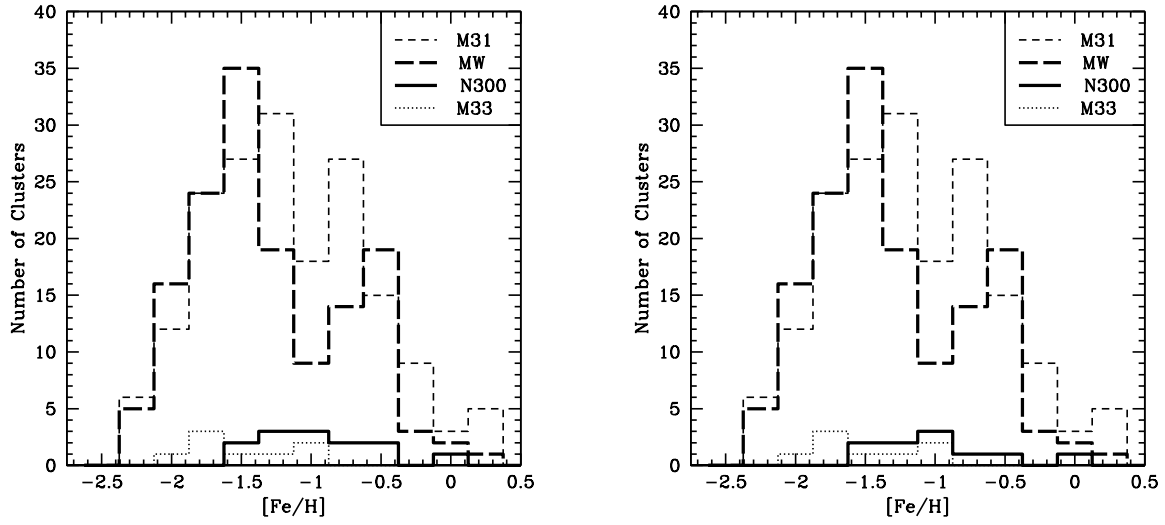


Fig. 13.— NGC 300 metallicity distributions, including (left) and not including (right) candidates flagged as possible stars. M31, M33, and Milky Way metallicity distributions are shown for comparison.

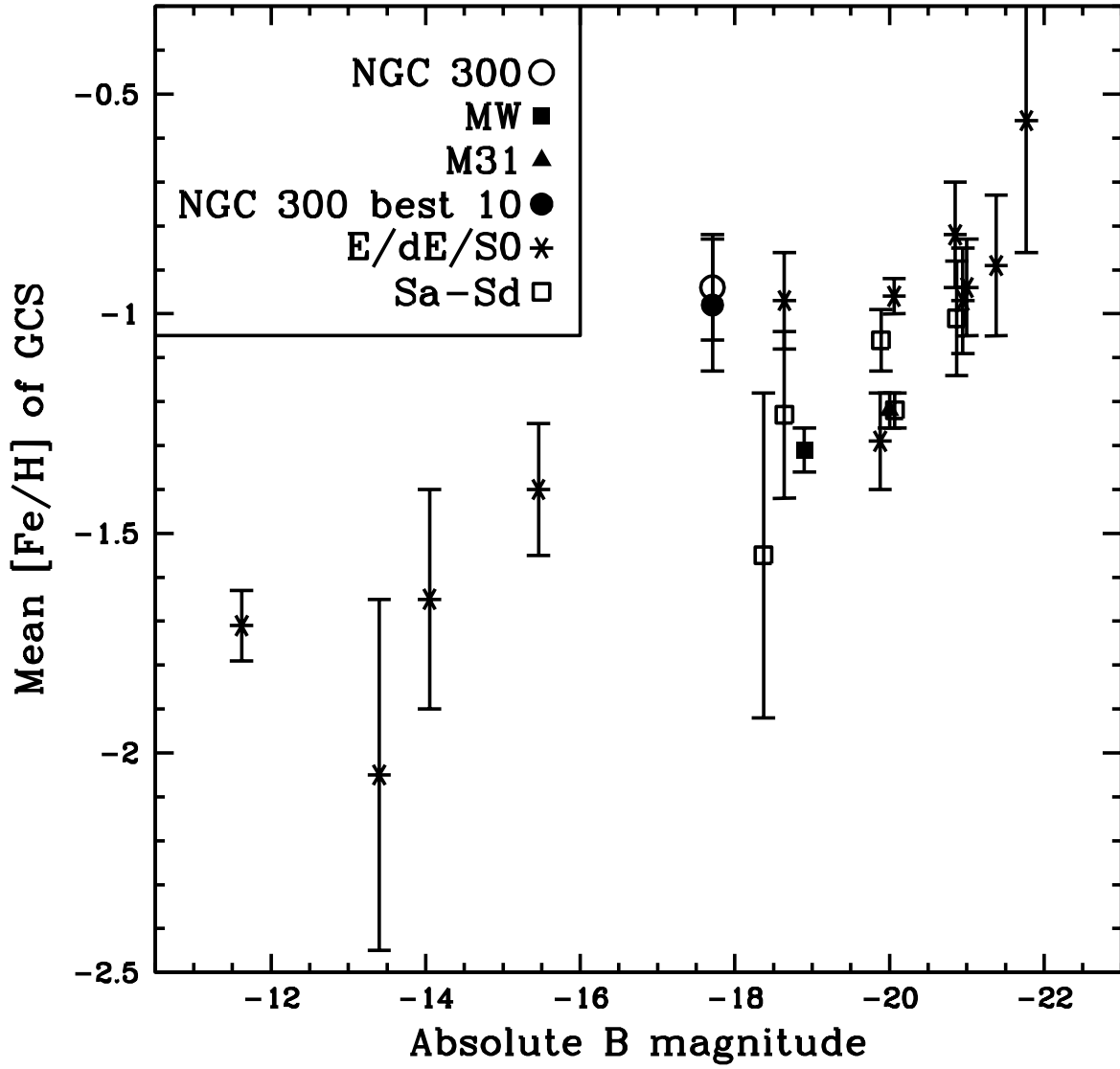


Fig. 14.— Average GCS metallicity vs. absolute B magnitude, showing NGC 300’s position including and excluding the low-velocity “GC or star” objects.

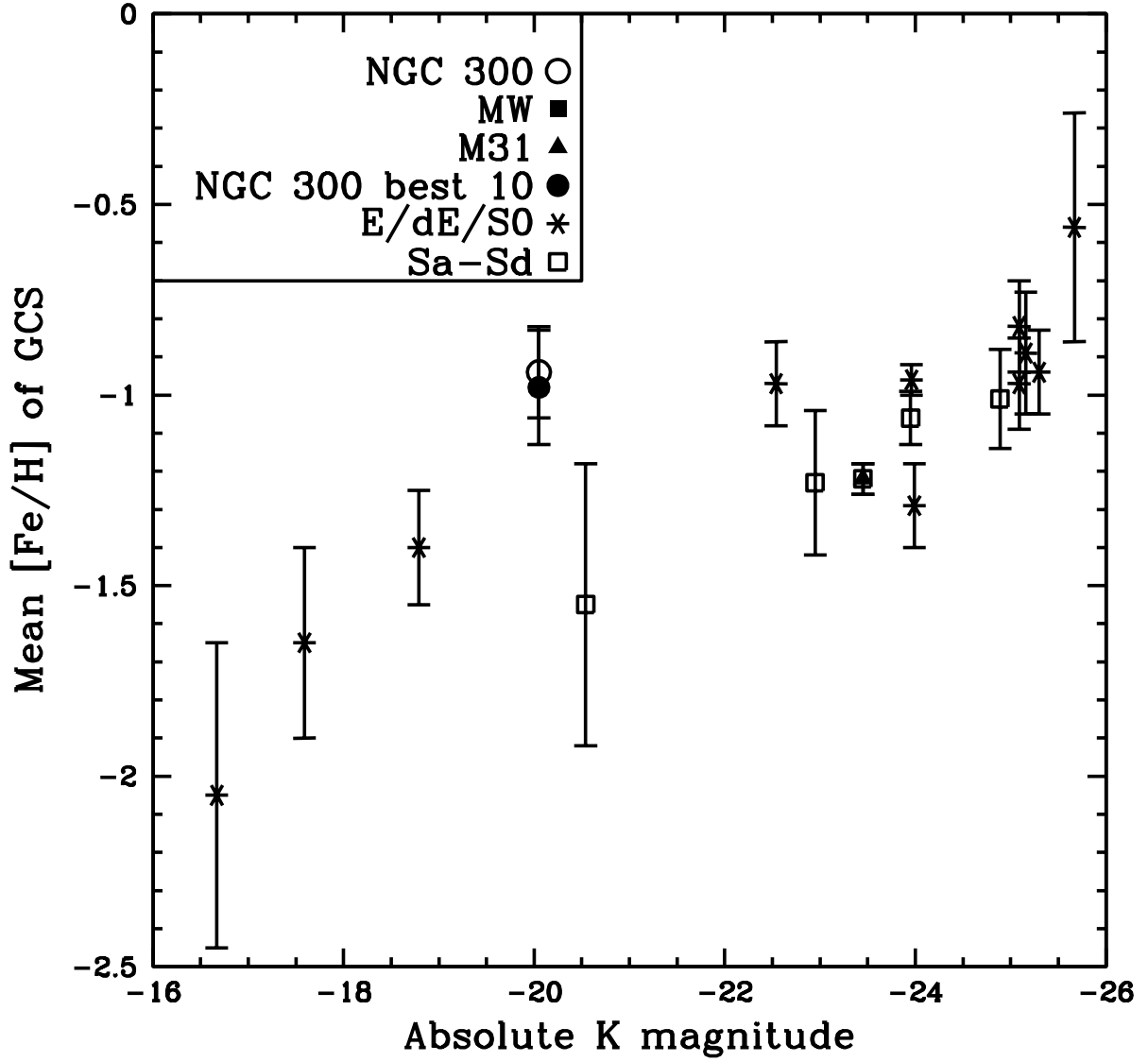


Fig. 15.— Average GCS metallicity vs. absolute K magnitude. Symbols are the same as in figure 8.

Table 1. Sculptor Velocities and Object Types from Spectra

Name	RA hh:mm:ss	DEC dd:mm:ss	K02 class	Velocity (km s ⁻¹)	Vel. err. (km s ⁻¹)	R-value	Template.	Object Type
NGC 253b	00:46:50.70	-25:26:38.90	–	209	43	7.87	m31_a_temp	gc
NGC 253ad	00:47:31.91	-25:26:42.53	–	65	40	7.42	fn4486btemp	gc
NGC 300cz	00:53:26.93	-37:41:55.54	–	81	19	16.6	fallstars	star
NGC 300cy	00:53:27.89	-37:55:21.48	–	85377	24	6.73	hemtemp0.0	(em.?)gal
NGC 300dt	00:53:40.30	-37:49:34.38	–	127	40	8.68	habtemp90	gc
NGC 300db	00:53:55.35	-37:23:42.98	–	-123	46	5.95	m31_f_temp	gc or star
NGC 300ds	00:53:56.12	-37:34:49.40	–	169	21	13.27	fabtemp97	star
NGC 300dd	00:53:56.47	-37:58:46.59	–	11483	29	4.26	hemtemp0.0	gal?
NGC 300cm	00:54:05.51	-37:42:06.11	–	-18	19	14.24	m31_k_temp	gc or star
NGC 300-01	00:54:22.07	-37:43:22.1	1	49374	34	8.78	habtemp90	gal*
NGC 300ck	00:54:21.84	-37:32:07.82	–	21	13	19.27	fallstars	gc
NGC 300cj	00:54:24.13	-37:25:46.17	–	23	17	15.63	m31_k_temp	gc
NGC 300-08	00:54:57.41	-37:33:55.30	2	16797	22	14.43	habtemp90	gal*
NGC 300-02	00:54:35.80	-37:43:05.60	2	59	21	15.11	habtemp90	gc
NGC 300-15	00:55:21.81	-37:45:40.10	2	106	22	20.12	m31_a_temp	star
NGC 300-03	00:54:40.02	-37:49:18.71	3	78	28	10.04	m31_f_temp	gc
NGC 300-04	00:54:45.62	-37:43:41.00	2	161	28	9.14	m31_f_temp	gc
NGC 300-14	00:55:17.67	-37:36:57.90	2	16995	36	8.68	fallstars	gal
NGC 300-05	00:54:49.35	-37:43:30.50	2	120	35	8.08	m31_f_temp	gc*
NGC 300-09	00:54:57.57	-37:36:37.90	2	214	14	18.08	fglotemp	star*
NGC 300-11	00:55:01.44	-37:37:21.80	1	38350	17	8.83	hemtemp0.0	em.gal*
NGC 300cl	00:54:53.85	-37:23:57.44	–	21	16	17.4	fabtemp97	star
NGC 300dc	00:54:54.66	-37:58:34.98	–	68066	25	5.13	hemtemp0.0	em.gal
NGC 300df	00:54:57.02	-37:58:52.21	–	-16	48	5.76	m31_k_temp	star
NGC 300-10	00:54:59.03	-37:36:24.40	3	173	23	12.59	m31_f_temp	star*
NGC 300ax	00:55:01.49	-37:47:36.40	–	-27	32	8.43	m31_k_temp	star
NGC 300-07	00:54:53.22	-37:43:11.1	1	43722	27	6.41	hemtemp0.0	em.gal*
NGC 300-12	00:55:11.03	-37:36:46.10	1	177	18	15.19	m31_f_temp	gc
NGC 300co	00:55:19.49	-37:29:38.73	–	-66	19	14.57	m31_k_temp	gc or star
NGC 300-06	00:54:51.67	-37:39:38.00	3	156	14	8.97	hemtemp0.0	HII*
NGC 300-17	00:55:38.79	-37:46:30.70	3	16868	21	13.02	fallstars	gal
NGC 300-16	00:55:27.56	-37:46:09.40	3	16798	29	8.03	m31_k_temp	gal
NGC 300-13	00:55:11.17	-37:33:13.90	3	38182	20	6.19	hemtemp0.0	em.gal
NGC 300cr	00:55:52.72	-37:59:04.14	–	-23	15	17.05	fallstars	star
NGC 300bd	00:55:56.79	-37:52:07.28	–	68818	20	6.69	hemtemp0.0	gal
NGC 300cq	00:56:07.09	-37:57:02.64	–	-79	14	17.25	fallstars	star
NGC 300cs	00:56:07.62	-37:57:23.07	–	31	16	15.85	fallstars	star
NGC 300da	00:56:09.49	-37:31:21.25	–	49619	21	7.51	hemtemp0.0	em.gal
NGC 300cv	00:56:13.97	-37:34:16.27	–	97	17	12.33	fabtemp97	star
NGC 300ct	00:56:18.24	-37:28:48.08	–	4	15	17.59	fabtemp97	star
NGC 300cp	00:56:19.03	-37:29:17.23	–	35	19	13.88	m31_k_temp	gc
NGC 300cx	00:56:20.30	-37:59:11.68	–	68618	53	5.97	m31_f_temp	gal
NGC 300cn	00:56:23.52	-37:27:37.57	–	49828	17	8.89	hemtemp0.0	em.gal
NGC 300cu	00:56:24.62	-37:52:56.29	–	18	20	12.33	fallstars	star

Note. — Objects with letter designations (e.g. NGC 300cx) are from Olsen et al. (2004). Objects with number designations (e.g. NGC 300-05) are from Kim et al. (2002). Objects with asterisks next to the object type have been visually inspected in archival HST images.

Table 2. Radial Velocities of Previously Observed GCs

ID	RA (J2000) (hours)	Dec (J2000) (minutes)	RV (km s ⁻¹)	σ_{RV} (km s ⁻¹)	Object type	Vel. source
NGC 300ac	00:54:02.48	-37:44:31.64	82	45	gc	Olsen et al. 2004
NGC 300ag	00:54:23.22	-37:59:17.67	120	38	gc	Olsen et al. 2004
NGC 300am	00:54:07.54	-37:42:09.23	73	17	gc	Olsen (unpublished)
NGC 300ba	00:54:05.49	-37:23:11.24	118	60	gc	Olsen et al. 2004
NGC 300m	00:54:07.04	-37:41:10.35	18	13	gc	Olsen (unpublished)
NGC 300r	00:56:23.13	-37:33:26.98	248	15	gc	Olsen et al. 2004
NGC 300s	00:53:55.66	-37:32:37.38	249	29	gc	Olsen et al. 2004

Table 3. Brodie & Huchra Calibrated Spectral Indices and H δ

Name	CNR mag	CH/G mag	H β mag	MgH mag	Mg2 mag	Mgb mag	Fe52 mag	NaI mag	CNB mag	H&K mag	MgG mag	δ mag	H δ A mag
NGC 253ad	0.017	0.262	0.039	0.048	0.177	0.152	0.027	0.046	0.294	0.312	-0.086	0.477	-0.83
σ	0.060	0.071	0.037	0.022	0.025	0.043	0.035	0.041	0.120	0.121	0.069	0.031	0.066
NGC 253b	-0.132	0.037	0.058	0.009	0.017	0.005	-0.005	0.049	0.216	0.234	-0.088	0.252	0.101
σ	0.042	0.053	0.033	0.020	0.022	0.037	0.033	0.042	0.071	0.067	0.050	0.019	0.045
NGC 300-02	-0.044	0.144	0.025	0.001	0.120	0.110	0.046	0.039	0.033	0.216	0.001	0.244	0.001
σ	0.011	0.015	0.010	0.006	0.007	0.012	0.010	0.013	0.020	0.019	0.015	0.005	0.012
NGC 300-03	-0.045	0.103	0.079	-0.008	0.018	0.045	-0.007	0.035	0.128	0.312	-0.188	0.298	0.048
σ	0.026	0.031	0.020	0.013	0.014	0.023	0.021	0.029	0.047	0.044	0.035	0.012	0.028
NGC 300-04	-0.015	0.120	0.063	0.010	0.037	0.064	0.066	0.008	0.095	0.328	-0.165	0.354	0.013
σ	0.031	0.037	0.023	0.014	0.015	0.026	0.023	0.030	0.058	0.057	0.040	0.015	0.034
NGC 300-05	-0.051	0.031	0.045	0.007	0.062	0.086	0.039	-0.047	-0.057	0.184	-0.134	0.243	0.090
σ	0.036	0.044	0.029	0.017	0.019	0.033	0.029	0.043	0.068	0.062	0.051	0.016	0.038
NGC 300-12	-0.053	0.138	0.071	0.030	0.101	0.088	0.056	0.026	0.069	0.362	-0.245	0.446	0.024
σ	0.018	0.023	0.013	0.008	0.009	0.015	0.013	0.016	0.036	0.034	0.026	0.009	0.020
NGC 300cj	-0.058	0.225	0.054	0.012	0.136	0.136	0.051	0.049	0.175	0.399	-0.187	0.536	-0.043
σ	0.014	0.018	0.010	0.006	0.007	0.012	0.011	0.012	0.026	0.025	0.018	0.007	0.014
NGC 300ck	-0.029	0.231	0.060	0.030	0.203	0.180	0.084	0.070	0.317	0.378	-0.200	0.664	-0.62
σ	0.016	0.021	0.012	0.007	0.008	0.014	0.012	0.013	0.032	0.029	0.023	0.008	0.017
NGC 300cm	-0.052	0.182	0.072	0.022	0.157	0.160	0.059	0.036	0.203	0.350	-0.108	0.483	-0.023
σ	0.018	0.023	0.014	0.008	0.009	0.016	0.014	0.016	0.034	0.033	0.023	0.009	0.019
NGC 300co	0.013	0.145	0.031	0.013	0.125	0.121	0.059	0.060	0.300	0.434	-0.181	0.561	-0.049
σ	0.019	0.024	0.014	0.009	0.010	0.017	0.014	0.016	0.037	0.035	0.025	0.009	0.020
NGC 300cp	-0.047	0.202	0.090	-0.001	0.152	0.166	0.071	0.027	0.142	0.375	-0.082	0.460	0.005
σ	0.021	0.028	0.017	0.010	0.011	0.019	0.017	0.020	0.040	0.039	0.028	0.010	0.022
NGC 300db	-0.071	0.262	0.092	0.002	0.078	0.114	-0.007	-0.026	-0.010	0.268	-0.022	0.226	0.002
σ	0.043	0.055	0.033	0.020	0.022	0.037	0.033	0.042	0.079	0.076	0.056	0.019	0.046
NGC 300dt	-0.006	0.200	0.059	0.008	0.117	0.177	0.037	0.087	0.065	0.268	-0.024	0.269	-0.052
σ	0.034	0.044	0.023	0.013	0.015	0.026	0.022	0.028	0.069	0.065	0.046	0.017	0.037
<NGC 300>	-0.038	0.165	0.062	0.011	0.109	0.120	0.046	0.030	0.122	0.323	-0.128	0.399	-0.004
σ	0.007	0.009	0.005	0.003	0.004	0.006	0.005	0.007	0.013	0.012	0.009	0.003	0.026

Note. — CNR \sim Lick/IDS CN1; MgH \sim Lick/IDS Index Mg1; NaI \sim Lick/IDS index NaD. All other indices correspond to the Lick/IDS indices of the same name. CNB, H&K, MgG, and δ have no Lick/IDS equivalents..

Table 4. Other Spectral Indices

Name	CN2 mag	Ca42 mag	Fe43 mag	Ca44 mag	Fe45 mag	C2 mag	Fe50 mag	Fe53 mag	Fe54 mag	Fe5709 mag	Fe5782 mag	TiO1 mag	TiO2 mag
NGC 253ad	0.041	0.102	0.088	0.048	0.056	0.060	0.052	0.036	0.036	0.058	-0.014	0.008	0.028
σ	0.076	0.106	0.066	0.067	0.055	0.042	0.037	0.044	0.045	0.038	0.045	0.024	0.023
NGC 253b	-0.104	-0.048	0.001	0.049	0.075	0.067	0.001	-0.029	-0.029	0.001	-0.021	-0.010	0.008
σ	0.055	0.076	0.052	0.053	0.046	0.036	0.033	0.042	0.042	0.037	0.043	0.024	0.023
NGC 300-02	-0.030	0.066	0.067	0.032	0.046	0.013	0.032	0.047	0.047	0.018	0.022	0.009	0.012
σ	0.015	0.020	0.014	0.015	0.013	0.011	0.010	0.013	0.014	0.012	0.015	0.008	0.008
NGC 300-03	-0.021	0.072	-0.020	0.023	0.081	0.024	0.046	-0.008	-0.008	0.019	-0.019	-0.032	0.007
σ	0.034	0.045	0.032	0.032	0.028	0.022	0.021	0.027	0.027	0.024	0.029	0.016	0.015
NGC 300-04	-0.026	0.072	0.060	0.028	0.069	0.044	0.065	0.052	0.052	0.038	0.024	0.007	0.011
σ	0.042	0.055	0.038	0.038	0.032	0.025	0.023	0.028	0.029	0.027	0.032	0.018	0.017
NGC 300-05	-0.052	0.081	-0.004	-0.045	0.003	0.012	-0.017	0.031	0.031	-0.025	-0.047	0.005	0.016
σ	0.049	0.062	0.045	0.047	0.040	0.031	0.030	0.036	0.037	0.036	0.043	0.024	0.023
NGC 300-12	-0.023	0.102	0.064	0.030	0.069	0.027	0.036	0.040	0.040	0.023	0.022	0.042	0.064
σ	0.024	0.032	0.021	0.023	0.018	0.015	0.014	0.017	0.017	0.015	0.018	0.010	0.010
NGC 300cj	-0.036	0.069	0.096	0.050	0.067	0.039	0.050	0.041	0.041	0.027	0.013	-0.009	0.009
σ	0.018	0.024	0.017	0.017	0.014	0.012	0.011	0.013	0.014	0.012	0.014	0.008	0.008
NGC 300ck	0.011	0.147	0.120	0.069	0.072	0.050	0.068	0.077	0.077	0.016	0.030	0.001	0.017
σ	0.020	0.028	0.018	0.019	0.016	0.013	0.012	0.015	0.016	0.013	0.016	0.009	0.009
NGC 300cm	-0.026	0.144	0.083	0.071	0.053	0.004	0.026	0.052	0.052	0.001	0.030	0.020	0.005
σ	0.023	0.032	0.021	0.022	0.019	0.015	0.014	0.017	0.018	0.016	0.019	0.010	0.010
NGC 300co	0.039	0.124	0.039	0.041	0.049	0.012	0.044	0.039	0.039	0.023	0.019	-0.001	0.008
σ	0.024	0.034	0.022	0.024	0.020	0.016	0.015	0.018	0.019	0.016	0.019	0.010	0.010
NGC 300cp	-0.009	0.110	0.039	0.045	0.055	0.038	0.037	0.044	0.044	0.001	0.023	-0.008	0.015
σ	0.027	0.038	0.026	0.027	0.022	0.018	0.017	0.021	0.022	0.019	0.023	0.012	0.012
NGC 300db	-0.043	0.091	-0.023	-0.004	-0.061	0.016	0.022	0.043	0.043	-0.025	-0.080	-0.058	-0.021
σ	0.056	0.074	0.055	0.057	0.048	0.037	0.034	0.041	0.042	0.038	0.046	0.024	0.025
NGC 300dt	0.000	0.131	0.134	0.088	0.063	-0.006	0.037	0.009	0.009	0.025	-0.048	-0.021	0.002
σ	0.044	0.056	0.036	0.037	0.032	0.025	0.022	0.028	0.028	0.025	0.030	0.016	0.016
<NGC 300>	-0.018	0.101	0.055	0.036	0.047	0.023	0.037	0.039	0.037	0.012	-0.001	-0.004	0.012
σ	0.009	0.012	0.008	0.009	0.007	0.006	0.005	0.007	0.007	0.006	0.007	0.004	0.004

Table 5. Linear Fits to $[Fe/H] = a(index) + b$

Index ID	a (dex/mag)	b (dex)	R^2	R_I	σ_m	σ_s
Ca4455	25.85	-2.00	0.899	0.0387	0.006	0.003
Fe5270	26.50	-2.31	0.888	0.0377	0.006	0.001
Mg2	9.83	-1.89	0.886	0.1017	0.017	0.006
δ	4.12	-2.68	0.884	0.2428	0.041	0.095
Fe5335	30.36	-2.22	0.879	0.0329	0.006	0.005
Ca4227	18.65	-2.09	0.878	0.0536	0.010	0.014
CN2	9.45	-1.27	0.852	0.1058	0.020	0.021
G4300	10.37	-2.24	0.844	0.0964	0.019	0.008

Table 6. Sculptor GC Metallicities

Name	[Fe/H] dex	$\sigma_{[Fe/H]}$ dex	[Fe/H] Src.	Ols. No.
NGC 55az	-1.76	0.43	Ols	27
NGC 253q	-1.07	0.30	Ols	5
NGC 253b	-1.96	0.54	new	26
NGC 247a	-1.04	0.29	Ols	64
NGC 253a	-0.88	0.25	Ols	46
NGC 253ad	-0.52	0.56	new	57
NGC 300dt	-0.89	0.66	new	13
NGC 300db	-1.23	0.81	new	22
NGC 300cm	-0.54	0.36	new	33
NGC 300ck	-0.07	0.25	new	42
NGC 300cj	-0.71	0.35	new	45
NGC 300-02	-1.03	0.29	new	n/a
NGC 300-03	-1.61	0.47	new	48
NGC 300-04	-1.18	0.33	new	n/a
NGC 300-05	-1.57	0.52	new	n/a
NGC 300-12	-0.93	0.23	new	n/a
NGC 300co	-0.67	0.29	new	69
NGC 300cp	-0.59	0.29	new	116
NGC 300r	-1.25	0.35	Ols	121

Note. — Ols.No. is the object number in Olsen et al. (2004) Table 4. Src. designates the source of the metallicity value: "Ols" for Olsen et al. (2004) or "new" for the newly reduced spectra.

Table 7. Mean Galaxy GCS Metallicities and Luminosities

ID	$\langle [m/H] \rangle$ (dex)	$\sigma_{\langle [m/H] \rangle}$ (dex)	B_t (mag)	Distance (Mpc)	M_{B_t} (mag)	K (mag)	M_K (mag)	Ref-Metal	Ref-Dist.	Ref-K
Fornax	-1.71	0.08	9.28	0.136	-11.38	–	–	32	5	–
M87	-0.89	0.16	9.56	15.631	-21.38	5.81	-25.16	6	11	17
M31	-1.22	0.04	4.36	0.77	-20.07	0.98	-23.45	2	12	17
MW	-1.31	0.05	5.52	0.76	-18.9	–	–	16	–	–
M81	-1.19	0.14	7.89	3.6	-19.89	3.83	-23.95	29, 26	13	17
M33	-1.55	0.37	6.27	0.847	-18.37	4.1	-20.54	6	14	17
M49	-0.56	0.3	9.37	16.368	-21.7	5.4	-25.67	9	11	17
N 147	-2.05	0.4	10.47	0.594	-13.4	7.2	-16.67	6	19	17
N 205	-1.40	0.15	8.92	0.752	-15.46	5.59	-18.79	6	30	17
N 185	-1.65	0.25	10.1	0.676	-14.05	6.56	-17.59	6	23	17
M104	-1.01	0.13	8.98	9.333	-20.87	4.96	-24.89	22	11	17
N 5128	-0.96	0.04	7.84	3.8	-20.06	3.94	-23.96	3	28	17
N 2683	-1.23	0.19	10.64	7.178	-18.64	6.33	-22.95	27	33, 18	17
N 7457	-0.97	0.11	12.09	13.996	-18.64	8.19	-22.54	8	11, 7	1
N 1023	-1.29	0.11	10.35	11.117	-19.88	6.24	-23.99	21	11	17
N 1399	-0.82	0.12	10	19.055	-21.4	6.31	-25.09	20	11	17
N 3923	-0.94	0.11	10.8	22.909	-21.0	6.5	-25.3	24	31	17
N 524	-0.97	0.12	11.3	28.2	-20.95	7.16	-25.09	4	10	1
N 300	-0.94	0.12	8.95	1.93	-17.48	6.38	-20.05	25, this paper	15	17

References. — (1) 2MASS Extended Source Catalog; (2) Barmby et al. 2000; (3) Beasley et al. 2008; (4) Beasley et al. 2004; (5) Bersier 2000; (6) Brodie and Huchra 1991; (7) Cappellari et al. 2006; (8) Chomiuk, Strader, and Brodie 2008; (9) Cohen, Blakeslee, and Coté 2003; (10) de Vaucouleurs et al. 1991; (11) Ferrarese et al. 2000; (12) Freedman 1990; (13) Freedman et al. 1994; (14) Galleti, Bellazzini, and Ferraro 2004; (15) Gieren et al. 2004; (16) Harris et al. 1996; (17) Jarrett et al. 2003; (18) Jensen et al. 2003; (19) Kang et al. 2007; (20) Kissler-Patig et al. 1998; (21) Larsen and Brodie 2002; (22) Larsen et al. 2002; (23) McConnachie et al. 2004; (24) Norris et al. 2008; (25) Olsen et al. 2004; (26) Perelmuter, Brodie, and Huchra 1995; (27) Proctor et al. 2008; (28) Rejkuba 2004; (29) Schröder et al. 2002; (30) Sharina, Afanasiev, and Puzia 2006; (31) Sikkema et al. 2006; (32) Strader et al. 2003; (33) Tonry et al. 2001.